J Atmos Chem (2018) 75:33–70
DOI 10.1007/s10874-017-9361-0

Measurements of PM_{10} ions and trace gases with the online system MARGA at the research station Melpitz in Germany – A five-year study

B. Stieger[1] · G. Spindler[1] · B. Fahlbusch[2] · K. Müller[1] · A. Grüner[1] · L. Poulain[1] · L. Thöni[3] · E. Seitler[3] · M. Wallasch[4] · H. Herrmann[1]

Received: 13 September 2016 / Accepted: 10 April 2017 /
Published online: 29 April 2017

Abstract An hourly quantification of inorganic water-soluble PM_{10} ions and corresponding trace gases was performed using the Monitor for AeRosols and Gases in ambient Air (MARGA) at the TROPOS research site in Melpitz, Germany. The data availability amounts to over 80% for the five-year measurement period from 2010 to 2014. Comparisons were performed for the evaluation of the MARGA, resulting in coefficients of determinations (slopes) of 0.91 (0.90) for the measurements against the SO_2 gas monitor, 0.84 (0.88), 0.79 (1.39), 0.85 (1.20) for the ACSM NO_3^-, SO_4^{2-} and NH_4^+ measurements, respectively, and 0.85 (0.65), 0.88 (0.68), 0.91 (0.83), 0.86 (0.82) for the filter measurements of Cl^-, NO_3^-, SO_4^{2-} and NH_4^+, respectively. A HONO comparison with a batch denuder shows large scatter (R^2 = 0.41). The MARGA HNO_3 is underestimated compared to a batch and coated denuder with shorter inlets (slopes of 0.16 and 0.08, respectively). Less NH_3 was observed in coated denuders for high ambient concentrations. Long-time measurements show clear daily and seasonal variabilities. Potential Source Contribution Function (PSCF) analysis indicates the emission area of particulate ions Cl^-, NO_3^-, SO_4^{2-}, NH_4^+, K^+ and gaseous SO_2 to lie in eastern European countries, predominantly in wintertime. Coarse mode sea salt particles are transported from the North Sea to Melpitz. The particles at Melpitz are nearly neutralised with a mean molar ratio of 0.90 for the five-year study. A slight increase of the neutralization

Electronic supplementary material The online version of this article (doi:10.1007/s10874-017-9361-0) contains supplementary material, which is available to authorized users.

✉ H. Herrmann
herrmann@tropos.de

[1] Atmospheric Chemistry Department (ACD), Leibniz Institute for Tropospheric Research (TROPOS), Permoserstraße 15, 04318 Leipzig, Germany

[2] Im Dammwald 21, 61381 Friedrichsdorf, Germany

[3] Research Group for Environmental Monitoring, Alte Jonastraße 83, 8640 Rapperswil, Switzerland

[4] German Federal Environment Agency, Wörlitzer Platz 1, 06844 Dessau-Roßlau, Germany

ratio over the last three years indicates a stronger decrease of the anthropogenically emitted NO_3^- and SO_4^{2-} compared to NH_4^+.

Keywords Atmospheric long-term measurements · MARGA · Instrument comparison · Source apportionment · Acidity investigation · Temporal variation

1 Introduction

Atmospheric processing of particles and their precursor gases from terrestrial, marine, and various anthropogenic primary and secondary sources determines the chemical composition and physical properties of particulate matter (PM). Varying meteorological conditions influence these physical and chemical properties in a very complex manner (Vecchi et al. 2007; Katzman et al. 2010), while the chemical composition of the gas and particle phase is the result of chemical conversions by gas phase, multiphase and heterogeneous reactions (Herrmann 2003; Hamed et al. 2010; Peter et al. 2010).

In Central Europe, a significant amount of particulate matter consists of inorganic ions, including nitrate (NO_3^-), sulphate (SO_4^{2-}), ammonium (NH_4^+), and chloride (Cl^-) (e.g., Neusüß et al. 2000; Spindler et al. 2013; Rogula-Kozlowska 2015). The quantification of these ions is predominantly performed by the standard method of filter sampling followed by offline analysis. Filter measurements offer the advantage of a widespread analysis of the chemical composition for the particle phase. However, sampling takes a long time (one to several days) and depends on the ambient PM concentrations; also, sampling may be subject to both positive and negative artifacts (Liu et al. 2014; Chow et al. 2015). It is essential to minimize such artifact formation and, additionally, investigate the change of pollutant concentrations at a higher time resolution for studying atmospheric processes.

Alternatives to particle measurements with a high time resolution are mass spectrometric systems, such as the Aerosol Mass Spectrometer (AMS) (e.g., Canagaratna et al. 2007) and the Aerosol Chemical Speciation Monitor (ACSM) (e.g., Ng et al. 2011). Both instruments offer the chemical analysis of major non-refractory ions within submicron particles.

To allow for the quantification of refractory and coarse mode ions, particles are collected in a Steam-Jet Aerosol Collector (SJAC) in which the particles grow to droplets within a supersaturated environment (Khlystov et al. 1995). To avoid artifacts by corresponding water-soluble trace gases, a wet chemical denuder is placed in front of the SJAC. This methodology is also used within the Particle-Into-Liquid-Sampler (PILS) (Orsini et al. 2003; Sorooshian et al. 2006). Furthermore, the dissolved gases within the aqueous solution of the denuder can be quantitatively analyzed. This is, for example, applied in the wet annular denuder systems AMOR (Ammonia Monitor RIVM) of the National Institute for Public Health and the Environment (Dutch RIVM) (Wyers et al. 1993; Volten et al. 2012) or AMANDA (Ammonia Measurement by Annular Denuder sampling with online Analysis) described by Whitehead et al. (2008), Milford et al. (2009) and von Bobrutzki et al. (2010) in order to measure ambient ammonia (NH_3) concentrations. Known instruments combining a denuder and SJAC are the GRAEGOR (Gradient of Aerosol and Gases Online Registrator) (Thomas et al. 2009) and the online Ambient Ion Monitor (AIM) (Ellis et al. 2011; VandenBoer et al. 2011; Markovic et al. 2012; Markovic et al. 2014; Sudheer et al. 2014; VandenBoer et al. 2014; Hsu and Clair 2015; Sudheer and Rengarajan 2015). Additionally, Trebs et al. (2004) used a denuder/SJAC system to perform aerosol measurements in the

Amazon Basin. By coupling gas and particle measurements, phase partitioning processes of semivolatile particles and secondary inorganic aerosol formation can be investigated.

The commercial Monitor for AeRosols and Gases in ambient Air (MARGA) uses the same sampling combination of a SJAC and a Wet Rotating Denuder (WRD). ten Brink et al. (2007) and ten Brink et al. (2009) introduced the "MARGA-sizer". These authors measured aerosols of different cut-off diameters at the meteorological tower of Cabauw in the Netherlands. In recent years, MARGA measurements were performed worldwide. Literature about MARGA measurements at different sites is summarized in Table 1.

With regards to available MARGA time series and measurement sites, long-term measurements of inorganic compounds in the gas and particle phase with a high time resolution are still missing for Central Europe. A typical reference site is the TROPOS research site in Melpitz, Germany. Daily PM_{10} filter measurements have been continuously performed at this site since 1992 (e.g. Spindler et al. 2013). Besides this, more intense measurement campaigns are performed. At this site, size-segregated impactor sampling (e.g. Herrmann et al. 2006) or online instrumentation like the AMS (Poulain et al. 2011; Poulain et al. 2014) were deployed. Measurements indicate that Melpitz is under the influence of different but quite specific air masses (Spindler et al. 2010; Spindler et al. 2013).

The present study intends to address two objectives. Firstly, we intend to follow water-soluble inorganic gases and PM_{10} particle composition by hourly time resolution in order to investigate diurnal variations. Secondly, we seek to evaluate the performance of the MARGA for a potential application at measurement sites within the German Federal Environment Agency (UBA). For this purpose, a large inter-comparison exercise was performed comparing the MARGA results with collocated and parallel measurements at the Melpitz site.

2 Measuring site and methods

2.1 Site description and meteorological parameters

Measurements were performed at the research station of the Leibniz Institute for Tropospheric Research (TROPOS) in Melpitz (12°56′E, 51°32′N, 86 m a.s.l.). This rural field site is situated on a meadow and is surrounded by agricultural and forested areas. The station is part of the EMEP-Level 3 network (Co-operative Programme for Monitoring and Evaluation of the Long-Range Transmission of Air Pollutants in Europe) and the GAW (Global Atmosphere Watch) programme of WMO (World Meteorological Organization). A more detailed site description is given in Spindler et al. (2004) and Spindler et al. (2013).

Two different wind directions mainly influence the Melpitz site (Spindler et al. 2004). The dominating west wind reaches Melpitz after crossing a large area of Western Europe and the city of Leipzig, located about 50 km downwind of the site. These air masses are of marine origin. The second main wind direction is from the east and is mostly related to dry continental and – especially in winter – anthropogenically polluted air masses from Eastern Europe (Spindler et al. 2013).

Meteorological parameters are measured at the Melpitz site with the following instrumentation. In order to measure temperature and precipitation, instruments from the R.M. Young Company, U.S.A. (PT1000 and rain gauge) are used; relative humidity is measured using the CS215 sensor by Sensirion AG, Switzerland; and wind velocity and direction is measured by a WindSonic by Gill Instruments, UK. Global radiation and barometric pressure are recorded by

Table 1 MARGA measurements in literature with sampling sites and main topics

Author(s)	Location	Main topics
ten Brink et al. (2007)	Cabauw, NL	Introduction of MARGA and measurements of size-distributions of inorganic ions (2002)
ten Brink et al. (2009)	Cabauw, NL	Measurements of size-distributions of aerosols, ratio of nitrate to sulphate (2002)
Du et al. (2010)	Shanghai, CN	Ammonium particle-to-gas conversion (2009)
Li et al. (2010)	Shanghai, CN	Agricultural fire impacts on the air quality in Shanghai, Summer Harvesttime 2009
Du et al. (2011)	Shanghai, CN	Measurements during haze pollution events in Shanghai (2009)
Schaap et al. (2011)	Cabauw, NL	Illustrating the benefit using data with high time resolution for model evaluation (2007 to 2008)
Ye et al. (2011)	Shanghai, CN	Role of ammonia on haze formation (2009)
Fu et al. (2012)	Shanghai, CN	Morphology, composition and mixing state of carbonaceous aerosol (2010)
Makkonen et al. (2012)	Helsinki, FI	Investigation of nitrogen in aerosol and gas phase and aerosol acidity (2009 to 2010)
Mensah et al. (2012)	Cabauw, NL	Aerosol measurements in 2008 and 2009
Behera et al. (2013)	Singapore, SG	Coupling among gases and secondary inorganic aerosols (2011)
Huang et al. (2013)	Shanghai, CN	Investigation of the aerosol evolution influenced by regional transport (2011)
Khezri et al. (2013)	Singapore, SG	Measurements in an industrialized area (2011)
Leng et al. (2013)	Shanghai, CN	Surface cloud condensation nuclei and aerosol activity (2010 to 2011)
Li et al. (2013)	Shanghai, CN	Role of chemical composition of PM on aerosol single scattering albedo (2010)
Phillips et al. (2013)	Kleiner Feldberg, DE	Influence of N_2O_5 on HNO_3 concentrations measured by alkali- and aqueous-denuder techniques (2012)
Wang et al. (2013a)	Shanghai, CN	Anthropogenic pollution and dust plume measurements (2010)
Wen and Chen (2013)	Jinan, CN	Measurements during firework events (2013)
Ye et al. (2013)	Shanghai, CN	Investigation of hygroscopic growth of urban aerosol (2009)
Zhang et al. (2013)	Shanghai, CN	Urban aerosol during World Expo 2010
Fan et al. (2014)	Lanzhou, CN	Crustal material versus secondary air pollution (2011)
Huang et al. (2014)	Honk Kong, HK	Characterization of $PM_{2.5}$, source investigation, receptor modelling study (2011 to 2012)
Jansen et al. (2014a)	Shanghai, CN	Impact of ammonia on PM_1 and visibility degradation (2012)
Jansen et al. (2014b)	Hangzhou, CN	Role of secondary inorganic aerosol in $PM_{2.5}$ during haze and fog (2012)
Kong et al. (2014)	Shanghai, Hangzhou, Guangzhou, CN	Observations of linearity between sulphate and nitrate in PM (2009 to 2011)
Leng et al. (2014a)	Shanghai, CN	Role of new particle formation on aerosol cloud condensation nuclei (CCN) activity (2012)
Leng et al. (2014b)	Shanghai, CN	Variations of CCN and aerosol activity during fog and haze events (2010)
Makkonen et al. (2014)	Hyytiälä, FI	Temporal cycles of NH_3, HONO and HNO_3 at a boreal forest site (2010 to 2011)
Rumsey et al. (2014)	North Carolina, US	Performance study of the MARGA (US Environmental Protection Agency's Clean Air Status and Trends Network, CASTnet) (2010)
Shi et al. (2014)	Shanghai, CN	Investigation on PM_1 (variability, formation/dissociation, impacts on visibility) (2012)
Zhou et al. (2014)	Shanghai, CN	Measuring and modelling aerosols for haze events (2008 to 2010)

Table 1 (continued)

Author(s)	Location	Main topics
Allen et al. (2015)	Centreville, US	Influence of dust, sea spray and acidity on nitrate aerosol (2013)
Griffith et al. (2015)	Hong Kong, HK	Influences of thermodynamic and chemical composition on $PM_{2.5}$ nitrate
Twigg et al. (2015)	Auchencorth Moss, GB	$PM_{2.5}$ and PM_{10} measurements (2006 to 2012)
Wang et al. (2015)	Shanghai, CN	Investigation of $PM_{2.5}$ pollution from 2011 to 2013
Zhou et al. (2015)	Hong Kong, HK	Measurements of oxalate at a suburban coastal site (2012 to 2013)
Chen et al. (2016)	Guangzhou, CN	Aerosol characteristics during rainy and cold air-dust weather
Rumsey and Walker (2016)	North Carolina, US	MARGA for gradient flux measurements of speciated nitrogen and sulfur (2012)
Wang et al. (2016)	Shanghai, CN	Meteorological influence on chemical composition of $PM_{2.5}$ (2011 to 2013)
Zhou et al. (2016)	Hong Kong, HK	MARGA for comparison of a single particle aerosol mass spectrometer (2013)
Tan et al. (2017)	Guangzhou, CN	Analysis of aerosol liquid water content (2014 to 2015)

a net radiometer CNR1 (Kipp&Zonen, The Netherlands) and a digital barometer (Vaisala, Germany), respectively.

2.2 Instrument description

2.2.1 MARGA

The hourly time-resolved quantification of water-soluble ions in PM_{10} (Cl^-, NO_3^-, SO_4^{2-}, NH_4^+, Na^+, K^+, Mg^{2+}, Ca^{2+}) and their corresponding trace gases (HCl, HONO, HNO_3, SO_2, NH_3) was realized by the commercial MARGA 1S ADI 2080 (Monitor for AeRosols and Gases in ambient Air, Applikon, The Netherlands) (ten Brink et al. 2007). An air pump draws air into a sample box after passing an inside Teflon-coated PM_{10} inlet (URG, Chapel Hill, located 5.5 m above ground) and a 3.5 m long polyethylene (PE) tube that are cleaned and replaced, respectively, at least every three month. The airflow of 1 m^3 hr^{-1} is controlled by a Mass Flow Controller (MFC, Brooks, USA). Within the sample box, the air flows laminarily through a WRD in which water-soluble gases diffuse into an absorbing liquid at pH = 5.7 (Keuken et al. 1988; Wyers et al. 1993), consisting of double deionized water (>18 MΩcm) and 10 mg l^{-1} hydrogen peroxide (H_2O_2) as an added biocide. The particles in the airflow pass the WRD, since their diffusion velocities are smaller than those of the gases, and reach the SJAC (Khlystov et al. 1995; Slanina et al. 2001). Within the SJAC, a supersaturation of water vapour causes the particle to grow into droplets. A cyclone collects the droplets containing the water-soluble inorganic ions. The aqueous samples of the WRD and the SJAC are continuously transported into the analytical box by two syringe pumps (25 ml). The gas and particle samples are both collected in the course of one hour. The samples are successively injected into two ion-chromatographs (IC) with conductivity detectors (Metrohm, Switzerland) for the online analysis of the anionic and cationic compounds in both phases. Lithium bromide is used as the internal standard. The volumes of the anion and cation injection loops are 250 μl and 500 μl, respectively. The anions are separated by a Metrosep A Supp 10 (75/4.0) column and a Na_2CO_3/Na_2HCO_3 (7 mM/8 mM) eluent. The intrinsic conductivity of the anion eluent has to be suppressed chemically using 0.35 M H_3PO_4. A Metrosep C4

(100/4.0) column and a 3.2 mM HNO_3 eluent are used to separate the cations. The measured concentrations are corrected to standard conditions (20 °C, 1013 hPa). The lower detection limits and the inaccuracy are given in the Electronic Supplementary Material (Table S1). Blank measurements act only as indicator for contaminations as well as performance check-up and are not subtracted from real samples. The results are shown in the Electronic Supplementary Material as averages for every compound in Table S2. As the MARGA in Melpitz is built in 2009, it is not possible to check the performance of the MARGA by an extra valve with an external calibration standard.

2.2.2 PM_{10} filter measurements

PM_{10} particles are collected using a high-volume sampler DIGITEL DHA-80 (Digitel AG, Hegnau, Switzerland) on preheated quartz fibre filters (Munktell, Type MK360, Sweden). The sampling time lasts 24 hours from midnight to midnight with an airflow of 30 m^3 $hr.^{-1}$. The blank and loaded filters are conditioned for a period of 48–72 hours at (20 ± 1) °C and a relative humidity of (50 ± 5)% before being weighed by a microbalance (Mettler-Toledo; AT 261). Filters are extracted into ultrapure water (>18 MΩcm). Two ion chromatographs (ICS-3000, Dionex, USA) in the laboratory analyze the anions (column AS 18, eluent KOH) and cations (column CS 16, eluent methane sulfonic acid), respectively. A conductivity detector performs the cation analysis, while a coupled conductivity/UV-VIS detector is used for anion detection. Consequently, daily concentrations of Cl^-, NO_3^-, SO_4^{2-}, NH_4^+, Na^+, K^+, Mg^{2+} and Ca^{2+} are available for the whole MARGA measurement period (Spindler et al. 2010; Poulain et al. 2011; Spindler et al. 2013).

2.2.3 SO_2 gas monitor

The gas analyzer APSA-360A (Horiba, Kyoto, Japan) measures sulphur dioxide (SO_2) concentrations every minute based on ultraviolet (UV) fluorescence during the five-year measurement period. The SO_2 molecules are excited by UV radiation of a xenon lamp and emit light in the 220–420 nm wavelength range. The intensity of the fluorescence is proportional to the concentration.

2.2.4 NH_3 cavity ring down spectroscopy (Picarro)

The Picarro G1103 gas analyzer (Picarro Inc., USA) measures hourly NH_3 concentrations in the air from January 2010 to October 2011. The measurement utilizes the Cavity Ring Down Spectroscopy (CRDS, Berden et al. 2000) methodology. Within a resonator, a laser emits light, which is reflected by two mirrors. Besides a very small transmittance of the mirrors, NH_3 absorbs the energy. Thus, after some time, the light intensity diminishes, and the intensity decay time can be used to quantify the concentration of NH_3 (von Bobrutzki et al. 2010).

2.2.5 NH_3 mini-denuder

Since April 2010, an integrating mini-denuder has been used for the quantification of NH_3. NH_3 diffuses on the walls of a citric acid coated denuder, in which a laminar airflow (0.43 m^3 per day) exists. The NH_3-content of the denuder was quantified by flow injection at the German Federal Environment Agency (UBA). The mini-denuders are provided by UBA and were changed weekly.

2.2.6 Rotating annular batch denuder

A rotating annular batch denuder was used for synchronous measurements of nitrous acid (HONO) and HNO_3, which were absorbed into ultrapure water (Wyers et al. 1993). The batch denuder is an open system without any tubes or inlet in order to transport air directly inside. After a sampling time of one hour, the liquid is pumped into an auto-sampler. The hourly samples were taken for several summer and autumn days in 2011 and 2012 and were analyzed offline via ion chromatography with conductivity detectors (ICS-3000, Dionex, USA) at TROPOS.

2.2.7 Mini-denuder and mini-filter module (Midefix)

Two Midefix assemblies consisting of a mini-denuder and mini-filter module each were used for the measurement of gaseous NH_3, SO_2 and HNO_3 as well as particulate NH_4^+, SO_4^{2-} and NO_3^- (Dämmgen et al. 2010a, b) and was provided and analyzed by the Research Group for Environmental Monitoring (FUB) in Rapperswil, Switzerland. The two Midefix units were coated with potassium hydroxide (KOH) and phosphoric acid (H_3PO_4) in order to detect both anionic and cationic compounds, respectively. The trace gases are transported in a laminar airflow (0.5 m^3 per day) and diffuse on the coating of a 22-cm-long glass tube. Particles were collected on the coated mini-filter. After a sampling period of two weeks, the concentrations of the gases and particles were determined by flow injection analysis via photometric detection (NH_3, NH_4^+) or ion chromatography. The Midefix unit was operated in Melpitz from November 2010 until February 2013.

2.2.8 Radial symmetric diffusive air sampler (Radiello®)

The commercialized radial symmetric diffusive sampler (Radiello®) measures gaseous compounds in the air. In this study, Radiello® samplers were used to determine NH_3. Diffusive and adsorbing surfaces in these samplers are cylindrical and coaxial. A diffusive cylinder consists of microporous sintered polyethylene of an external diameter of 8 mm, a thickness of 1.7 mm, and an average porosity of 25 μm. It is coupled to an adsorbing cartridge with a radius of 2.9 mm, which is coated with H_3PO_4. The two parts create a fixed distance that forms the diffusive path. The diffuse sampler was installed in a suspension device, which was simultaneously acting as a shelter against the weather. After an exposition time of two weeks, the diffusive sampler was analyzed via flow injection with UV detection (Dämmgen et al. 2010a) by the FUB. Data were available for one year starting in February 2012.

2.2.9 ACSM

The Aerosol Chemical Speciation Monitor (ACSM, Aerodyne Inc., USA) analyzes the near PM_1 chemical composition at Melpitz since June 2012. A more detailed description of the ACSM is given by Ng et al. (2011). After passing through the instrument inlet, the sampled air is focused into a narrow beam by an aerodynamic lens. The focused particle beam then reaches the vaporization and ionization chamber where the non-refractory part of the particles is vaporized by impaction on a surface heated to 600 °C. Nearby, an electron impact ionization source (70 eV) ionizes the vaporized particles before entering a quadrupole mass spectrometer. The scan of the mass-to-charge ratio covers the range of 12 to 148 amu and the time resolution of the ACSM is approximately 30 min.

2.3 Trajectory calculation and source contribution modelling

To generate 96 hours backward trajectories, the Hybrid Single-Particle Lagrangian Integrated Trajectory (HYSPLIT) model was used (Stein et al. 2015). The trajectories were calculated for every hour for the entire measurement period of the MARGA starting at 500 m a.s.l.

The trajectories were combined with hourly MARGA data and the Potential Source Contribution Function (PSCF) is applied (Malm et al. 1985; Pekney et al. 2006; Xie and Berkowitz 2007; Hopke 2016) in order to study the most probable emission areas of the measured gases and PM_{10} compounds,. For every grid cell (*i,j*), the PSCF value is calculated by Eq. (1):

$$\mathrm{PSCF} = \frac{m_{ij}}{n_{ij}} \tag{1}$$

where n_{ij} is the number of all trajectories that passes the grid cell (*i,j*), and m_{ij} is the number of trajectories that show relatively high concentrations while passing the grid cell. The latter number can be varied by the use of different percentiles depending on the concentration course of the measured components. During the previous work, the 75*th* percentile was chosen for all species. Grid cells that have a lower number of trajectories were corrected by a weighting factor to reduce their effect. This calculation was performed using the software *R* (Mair et al. 2015) with the open access program package *'Openair'* (Carslaw and Ropkins 2012).

3 Results and discussion

3.1 Measurement period

Ion detections of 80% were achieved for the gases (HONO, HNO_3, SO_2, and NH_3) and the main ions (NO_3^-, SO_4^{2-}, NH_4^+) for the entire measurement period in Melpitz from 2010 until 2014. The single detection frequencies for every species are listed in Table 2. The low data coverage of the cations except NH_4^+ is attributed to concentrations below the detection limit in the hourly samples.

In autumn 2010, the MARGA participated in the HCCT 2010 campaign in Goldlauter for two months (Tilgner et al. 2014) and in an international CEN (European Committee for Standardization) field measurement campaign at the UBA site, Waldhof, from May until July 2014. Further data losses appeared due to maintenance and technical issues. For Mg^{2+} and Ca^{2+}, the years 2010 and 2011 were deleted due to artifact formation (compare section 3.2.2).

3.2 Comparison of the MARGA measurements with other methods

In this study, several comparisons of the MARGA with other instruments were executed. As an overview of the duration of the single comparisons in the following section, Fig. 1 shows the realized measurement for each instrument.

As many instruments have time resolutions different to the MARGA, it is necessary to adjust the MARGA concentrations or vice versa. E.g., to obtain the diurnal concentration, the mean of the hourly MARGA data was calculated with the requirement that at least 75% of the

Table 2 Ion detection of the gases and particulate ions for the MARGA measurement period from 2010 to 2014 in Melpitz

Gas / Particulate Ion	Ion detection [%]
HCl	51.4
HONO	81.0
HNO_3	80.8
SO_2	81.2
NH_3	78.0
Cl^-	52.4
NO_3^-	83.2
SO_4^{2-}	82.6
Na^+	30.0
NH_4^+	81.6
K^+	15.2
Mg^{2+}	10.5
Ca^{2+}	25.9

averaged data per day are available and lie above the lower detection limit. Otherwise, we do not consider the diurnal concentration.

3.2.1 Comparison of gas phase measurements

SO_2 The measurements using the MARGA system and the SO_2 gas monitor in parallel for five years show a coefficient of determination of $R^2 = 0.91$ and a slope of 0.90. The results in Fig. 2a demonstrate that a trustworthy measurement of SO_2 with the MARGA is possible for the whole concentration range. In Fig. 2b, a similar agreement can be achieved for the comparison with the mini-denuder unit of the Midefix for the two-year measurement period (slope 0.98, $R^2 = 0.73$). These results agree with those of Rumsey et al. (2014) for the comparison with a coated denuder.

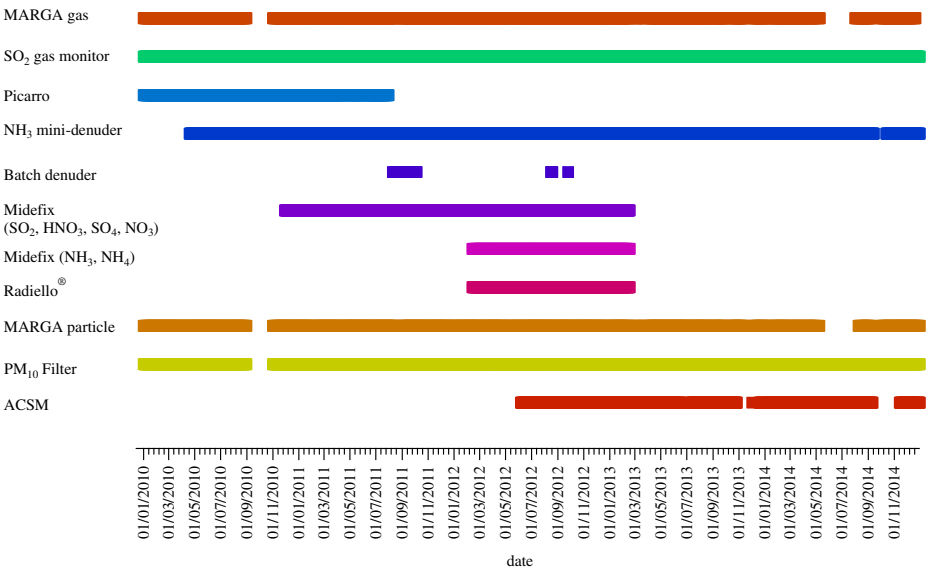

Fig. 1 Overview of the measurement periods for the different instruments at the Melpitz site

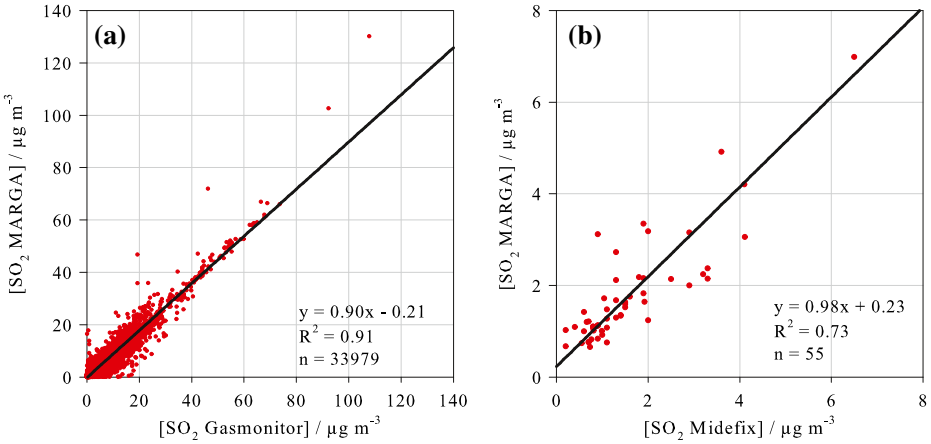

Fig. 2 Comparisons of SO_2 MARGA measurements (*y-axis*) with (**a**) the SO_2 gas monitor and (**b**) the Midefix, orthogonal regression (*black line*)

HONO The comparison of a rotating annular batch denuder with the MARGA for HONO measurements in Fig. 3 results in a slope of 1.10 and shows a large scatter field (R^2 = 0.41). Acker et al. (2004) used a wet effluent diffusion denuder (WEDD) and a rotating wet annular denuder (RWAN) for an eight-day comparison; the latter is similar to the WRD that is part of the MARGA. Pure water and a 0.0005 M K_2CO_3 solution were chosen as denuder liquids, respectively. These authors found analogous results with a slope of 1.028 and a coefficient of determination of R^2 = 0.63. Also, Genfa et al. (2003) compared two denuders (rotating wet annular denuder and wet parallel plate denuder with Na_2CO_3 and H_2O_2 solutions acting as absorbers, respectively) during the Atlanta Supersite study 1999 and found a coefficient of determination of 0.78 with a slope near

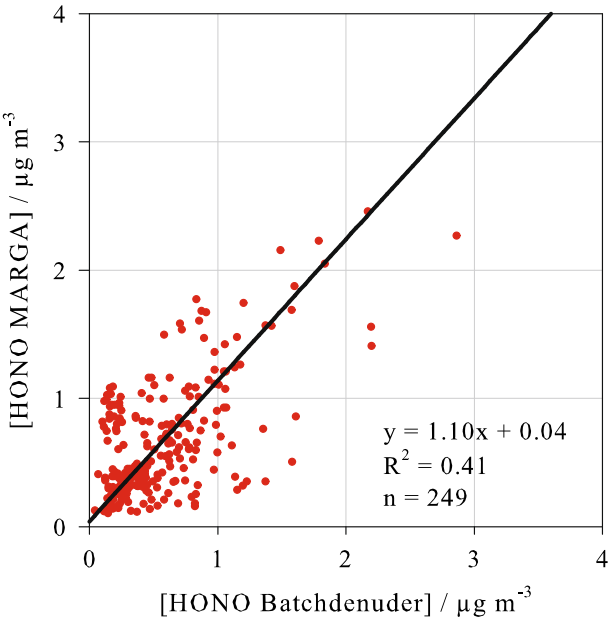

Fig. 3 Comparison of HONO measurements with the MARGA and the rotating annular batch denuder, orthogonal regression (*black line*)

unity. Absorber liquids with different pH values could explain the scattering in both studies. Spindler et al. (2003) used alkaline denuders and found several positive artifacts that could appear due to heterogeneous interactions of NO_2 and H_2O as well as reaction of NO_2 and SO_2 in water. In addition, the HONO sampling efficiency can be increased by the use of alkaline absorber solutions. In the present work, the compared denuders have the same pH of 5.7. A cause for the weak correlation could be found in the offline analysis for the batch denuder and in the heterogeneous and liquid phase reactions, which could slightly vary for each denuder. The additional H_2O_2 in the MARGA denuder could influence such reactions as well.

Stutz et al. (2010) mentioned that HONO measurements using most of the in-situ methods are problematic. Denuder techniques can measure higher values than optical measurement systems, such as, e.g., the Differential Optical Absorption Spectroscopy (DOAS). This is due to the fact that heterogeneous reactions on the wet surfaces can form additional nitrite (Kleffmann and Wiesen 2008). However, previous works of Spindler et al. (2003) and Acker et al. (2006) found agreements between the chemical denuder technique and the DOAS. Spindler et al. (2003) showed a relatively good agreement between both methods but also took into account the different measurement methods of both techniques. The denuder measures the concentration at one point whereas the DOAS is an integrating system that works over a long distance (several hundred meters). In the nighttime, a HONO gradient can be formed due to the appearance of an inversion layer. If the integrating path of the DOAS crosses different heights, a comparison with the point measurement of a denuder is difficult. Therefore, Acker et al. (2006) compared the DOAS and a denuder (here with a neutral absorbance solution) during well-mixed atmospheric conditions with the result of successful high-time resolved, sensitive, and comparable measurements of HONO. However, the cited authors also concluded that spectroscopic methods like DOAS show advantages when studying reactive species as HONO. Wang et al. (2013b) described the DOAS as highly selective, free of chemical interferences, and (in case of a well-mixed atmosphere) free of sampling artifacts.

HNO_3 The MARGA system was compared for HNO_3 with similar denuder instruments. Both the rotating annular batch denuder (slope = 0.16, R^2 = 0.45) and the denuder unit of the Midefix (slope = 0.08, R^2 = 0.06) show clear deviations from the measured HNO_3 concentrations by the MARGA (Fig. 4a,b).

An obvious underestimation of HNO_3 by the MARGA is observed in the comparison. The most likely reason is the "sticky" behavior of HNO_3 (Rumsey et al. 2014). While the sampled air is directly pumped in the rotating annular batch denuder and the Midefix, the inlet and the WRD of the MARGA are connected through a 3.5 m long PE tube in which HNO_3 can adsorb onto the walls. Neuman et al. (1999) compared different tubing materials for HNO_3 measurements in the laboratory, with the result that the least adsorption occurs using a perfluoroalkoxy (PFA) Teflon tubing above 10 °C. However, it was remarked that a high relative humidity strengthens the adsorption, which is often in conflict with field measurements. Regarding the comparison of the denuder instruments, the best solution would be to draw air directly into the MARGA system without an inlet. However, this would lead to a direct penetration of particles larger than 10 μm, and a strong influence of the prevailing meteorological conditions (e.g., frost and rain) could very quickly damage the MARGA system. Additionally, positive artifacts can occur for the HNO_3 detection by the MARGA system due to the heterogeneous reaction of N_2O_5 to HNO_3 mainly during nighttime (Phillips et al. 2013). This group found high sensitivities to N_2O_5 for wet chemical denuders and alkaline denuders. As the latter effect

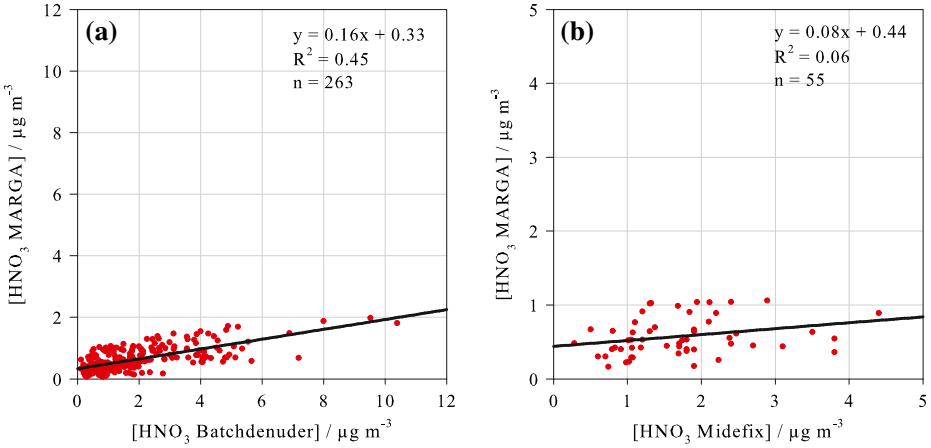

Fig. 4 Comparison of HNO_3 measurements with the MARGA (*y-axis*) and (**a**) the rotating annular batch denuder and (**b**) Midefix, orthogonal regression (*black line*)

would occur in all denuders in this comparison, it is not the reason for the observed underestimation of the MARGA HNO_3 measurement.

NH_3 Similar to HNO_3, a comparison of NH_3 MARGA measurements with other sampling instruments is essential as NH_3 can interact with the walls of the inlet due to its "sticky" behavior (von Bobrutzki et al. 2010). Norman et al. (2009) noted that cooling on the outside of the inlet can favour condensation within the tubing. This could lead to an adsorption of NH_3. It was suggested that the best way to avoid condensation is heating the inlet to some small amount above the ambient temperature. In Melpitz, a pipe enclosing the sampling tube is continuously ventilated to avoid cooling processes by rain and lower temperatures outside the air-conditioned container. Additionally, the high flow rate of the MARGA shortens the residence time of gaseous NH_3 inside the inlet tube and reduces the wall interactions. Whitehead et al. (2008) found that PE is the best material for the sampling of NH_3. The results of the comparisons in this work indicate that a wall loss of NH_3 is negligible due to higher MARGA concentrations compared to other instruments.

Volten et al. (2012) compared miniDOAS and AMOR, the latter using similar sampling methods as the MARGA. Both instruments had a time resolution of one minute. For high time resolutions, the authors found, firstly, a delay of the peaks in the AMOR data due to the turnover time of the liquid inside the denuder. Secondly, the AMOR could reach neither very low nor very high NH_3 concentrations. It was guessed that this could likely be the result of adsorption and desorption of NH_3 in the inlet. Daily averages of both instruments show a good agreement for the NH_3 variations, but with higher AMOR NH_3 concentrations due to possible memory effects in the inlet. Thus, in this work a memory effect for the MARGA should always be considered.

In Figs. 5 and 6, the comparison of the MARGA with the optical Picarro system bares discrepancies in the measurement of NH_3 ($R^2 = 0.50$). The Picarro detects up to 3 µg m^{-3} more NH_3 than the MARGA for low NH_3 concentrations (< 5 µg m^{-3}). This behavior could be explained by the use of a prefilter system in the Picarro instrument in order to avoid the penetration of particles into the sensitive resonator. Ammonium nitrate (NH_4NO_3) deposits onto the inlet filter surface and can afterwards evaporate due to its semi-volatility, depending

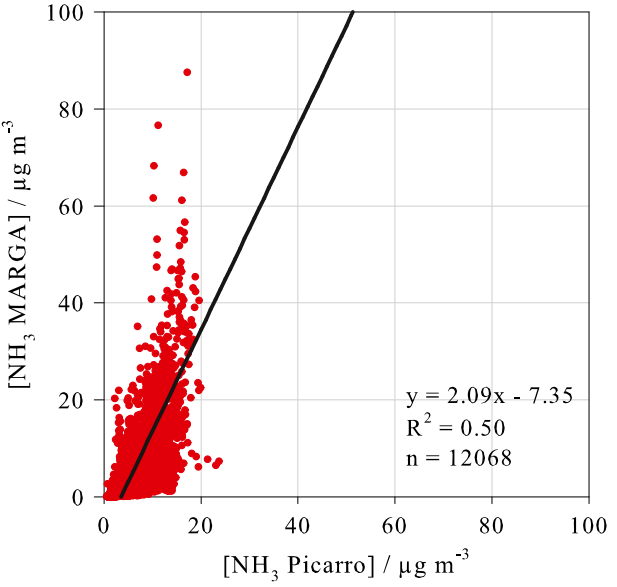

Fig. 5 Comparison of NH_3 measurements with the MARGA and the Picarro gas analyzer based on cavity ring down spectroscopy with orthogonal regression (*black line*)

on ambient temperature and relative humidity (Schaap et al. 2004; Keck and Wittmaack 2005; Plessow et al. 2005). The evaporated gaseous NH_3 is then measured by the Picarro system, leading to higher concentrations compared to the concentrations measured with the MARGA directly. This could explain the negative intercept of −7.35. For higher NH_3 concentrations, an opposite behavior is recognizable. For NH_3 concentrations greater than 15 µg m^{-3}, the Picarro system shows a significant underestimation (Fig. 6). A possible reason could be the formation of negative artifacts due to the prefilter. Acidic particles collected on the prefilter could lead to a significant loss of alkaline gaseous NH_3. In addition, the Picarro shows a very slow decrease after the detection of high NH_3 concentrations. During this time, the MARGA shows a much faster decrease with sharp peaks and more fluctuations. This sluggish behavior of the CRDS method is a result of the combination of both Picarro artifacts. Adsorbed NH_3 desorbs when

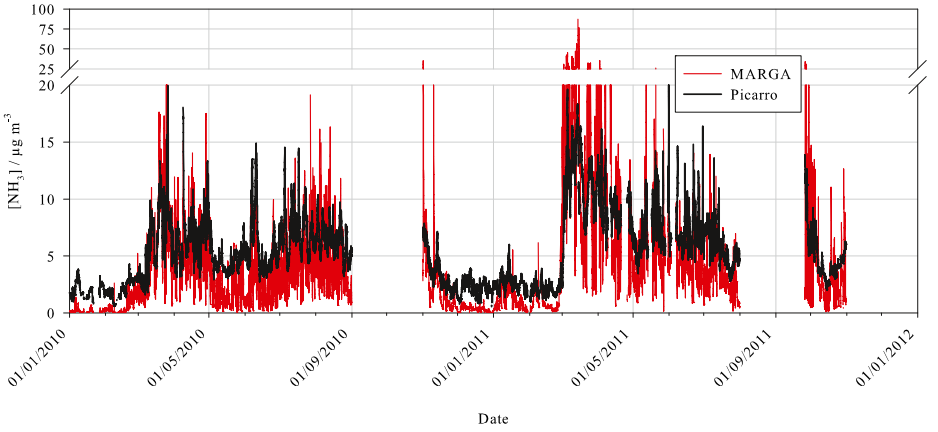

Fig. 6 Comparison of NH_3 measurements with the MARGA (*red*) and the Picarro gas analyzer (*black*) for the comparison period

higher temperatures or lower humidities and lower environmental NH_3 concentrations are given. The similar artifact with a prefilter was also mentioned by von Bobrutzki et al. (2010).

A comparison of different NH_3 measurement techniques by Schwab et al. (2007) suggests that denuder measurements show a very long time response. However, the NH_3 concentrations were measured every second via a fluorescence method and were reported as minute averages. The hourly MARGA data do not provide this high time resolution and a long time response cannot be observed.

As opposed to the MARGA NH_3 data comparison with the Picarro NH_3 measurements, the chemical analysis of the coated surfaces (NH_3 mini-denuder, Midefix and Radiello®) show better correlations. Those are summarized in Table 3. However, the slopes from 1.30 to 1.53 show that concentrations measured by coating techniques are generally lower than those of MARGA. In times of high NH_3 concentrations, these instruments measure less NH_3 than the MARGA. Regarding the diffuse samplers, it could be possible that the duration time is too short in times of high or strongly fluctuating concentrations. Nevertheless, the maximal saturation of the Radiello® is around 500 $\mu g\ m^{-3}$ for a biweekly exposition, which was never exceeded during the comparison period.

In contrast, Rumsey et al. (2014) observed higher NH_3 concentrations for the coated denuder measurements, which were sampled every 12 h. The cited authors try to explain their slopes with the "sticky" property of NH_3, similar to HNO_3, as well as variability in the denuder blank and possible inaccuracy of the external standard offset (Rumsey et al. 2014). Possibly, the different slopes can be explained by the fact that the measured NH_3 concentrations in this work were up to 10 times higher than the measured NH_3 by Rumsey et al. (2014).

Norman et al. (2009) compared the MARGA related GREAGOR system with an Automated Ammonia Analyzer (AiRRmonia) and a modified Proton Transfer Reaction Mass Spectrometer (PTR-MS) for five days of data. It was concluded that all instruments are suitable for atmospheric NH_3 measurements. In addition, von Bobrutzki et al. (2010) found good long-term stability for wet chemistry instruments.

3.2.2 Comparison of particle phase measurements

MARGA vs. ACSM The parameters for the orthogonal regressions for the comparison of the MARGA with the ACSM are summarized in Table 4. It should be noted again that different cut-off diameters for the particle composition analysis were used for the MARGA (PM_{10}) and the ACSM (PM_1). For SO_4^{2-} and NH_4^+, slopes of 1.39 and 1.20 were achieved, respectively. This indicates that there is a larger fraction of both ions in the coarse mode (PM_1-PM_{10}).

Higher NO_3^- concentrations were detected by the ACSM in comparison with the MARGA. The slope (0.88) is comparable with the study of Makkonen et al. (2014) (0.819), where a MARGA was compared with an AMS, which used a similar sampling and detection

Table 3 Overview of the orthogonal regressions for the comparisons with the MARGA and other denuder based NH_3 measurement instruments. The scatter plots can be found in the Electronic Supplementary Material (Fig. S1)

Instrument	Coating	Slope	Intercept	R^2	n
NH_3 mini-denuder	Citric acid	1.53	−0.05	0.82	179
Midefix	Phosphoric acid	1.30	−0.16	0.90	26
Radiello®	Phosphoric acid	1.44	−0.78	0.98	26

Table 4 Overview of the orthogonal regression parameters of NO_3^-, SO_4^{2-}, and NH_4^+ for the comparison of MARGA with the ACSM. The scatter plots are shown in the Electronic Supplementary Material (Fig. S2)

Ion	Slope	Intercept	R^2	n
NO_3^-	0.88	0.39	0.84	12,616
SO_4^{2-}	1.39	−0.19	0.79	12,480
NH_4^+	1.20	−0.12	0.85	12,527

technology as the ACSM (Ng et al. 2011). As suggested by Makkonen et al. (2014), this offset could be explained either by the measurement of organic nitrates with the ACSM/AMS or a lower response of the MARGA for these compounds. For periods of low NO_3^- concentrations, those measured by the MARGA tend to be slightly higher (intercept: 0.39).

Both instruments agree, but there are periods when the MARGA strongly overestimates the ACSM NO_3^- concentration (Fig. 7). During the 1st, 6th, 7th, 15th, and 16th September 2012, the site was influenced by westerly winds that transport marine air masses to the sampling site, as it can be illustrated by looking at the increase of the sodium concentration during these days. Therefore, the measured nitrate might not only include ammonium nitrate but also sodium nitrate ($NaNO_3$), resulting in the reaction of sodium chloride (NaCl) with HNO_3 when marine air masses crossed some polluted areas (Finlayson-Pitts and Pitts 1986; Pio and Lopes 1998). Similar to sea salt, $NaNO_3$ is a very low-volatile compound that evaporates at temperatures above 600 °C; therefore, it is quite difficult to detect this salt by ACSM. Moreover, $NaNO_3$ is principally present in the coarse mode, which is out of the ACSM size range. Consequently, the discrepancy between the two instruments during marine air mass influence might result in a size cutting effect, while it may also indicate the presence of two types of nitrate salts.

Some comparisons between AMS and MARGA or MARGA-related instruments were described. Mensah et al. (2012) compared a so-called "MARGA-sizer" with which various particle sizes can be analyzed. For the 1-μm channel of the MARGA-sizer, the measured concentrations of the different ions were on average a factor of 1.6 higher in comparison to the AMS. Better ratios could be achieved with the 0.56-μm channel, but the coefficients of determination decreased. The cited authors concluded that the deviations between the AMS and the MARGA-sizer are possible due to the different sample heights and potential losses

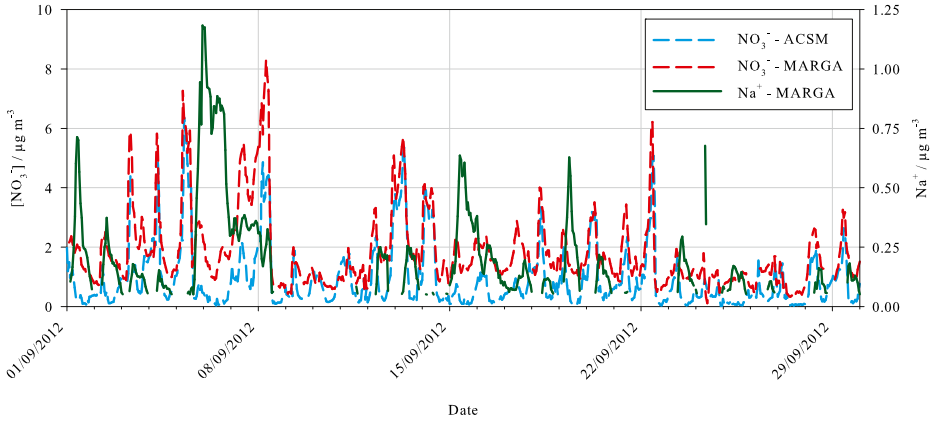

Fig. 7 Time course of NO_3^- as hourly values measured by the MARGA (*red*, PM_{10}) and ACSM (*blue*, PM_1) as well as MARGA Na^+ (*green*, PM_{10}) for September 2012

within the inlet. Markovic et al. (2012) compared the AMS with an Ambient Ion Monitor-Ion Chromatograph (AIM-IC) with a $PM_{2.5}$ inlet. For all ions, more highly averaged mass loadings were detected with the AMS. The authors hypothesized that if all particles are found in PM_1 and not all compounds are solved in water, then the AMS measures higher concentrations. Additionally, two more explanations were mentioned. First, the AMS data were corrected by the collection efficiency. Second, the collection efficiency for particles of the AIM-IC was lower than 100%. Nevertheless, this study and both mentioned groups conclude a qualitatively good agreement between MARGA and AMS (Mensah et al. 2012) as well as accurate measurements of the particulate NO_3^-, SO_4^{2-}, and NH_4^+ with the AIM-IC (Markovic et al. 2012).

MARGA vs. filter measurements Table 5 shows the results of the orthogonal regression of the data for the measurement period.

For the PM_{10} filter, coefficients of determination of 0.85–0.91 were obtained for the ions Cl^-, NO_3^-, SO_4^{2-} and NH_4^+. Slopes from 0.65 to 0.83 indicate an underestimation of the concentration by the MARGA compared to filters. A possible reason for this could be the adsorption of their gaseous forms onto the filter surface, whereby the offline analysis detects higher amounts of these ions. However, for NO_3^-, a converse behavior can be observed, as shown in Fig. 8a,b. The correlation for NO_3^- varies between summer (April–September; $R^2 = 0.76$, slope = 0.66) and winter (October–March; $R^2 = 0.88$, slope = 0.71). In summer, when the absolute concentration of nitrate is lower than in winter, a negative artifact exists for the filter sampling. This is because of the high volatility of NH_4NO_3 (Schaap et al. 2004; Keck and Wittmaack 2005; Plessow et al. 2005), that evaporates to NH_3 and HNO_3 during higher temperatures and lower humidities in summer. The ACSM data are also shown in Fig. 8a, b. In summer, the ASCM shows higher NO_3^- values compared to the filter, although the ACSM collects a smaller size fraction. In winter, the analysis of the PM_{10} filter shows slightly higher concentrations compared to MARGA and ACSM.

Interestingly, the slope between MARGA and Midefix for NO_3^- is close to unity (0.91) with nearly the same coefficients of determination. The Midefix was operated from November 2010 to February 2013 and covered two winters and summers. A summer/winter dependence

Table 5 Parameters of the orthogonal regression of the MARGA comparison with the daily PM_{10} filter measurements and the biweekly Midefix data. MARGA data were averaged per day and two weeks, respectively, with the requirement of at least 75% data coverage. The single scatter plots are shown in the Electronic Supplementary Material for the PM_{10} filter (Fig. S3) and Midefix (Fig. S4)

Instrument	Ion	Slope	Intercept	R^2	n
PM_{10} filter	Cl^-	0.65	0.08	0.85	710
	NO_3^-	0.68	0.56	0.88	1488
	SO_4^{2-}	0.83	0.02	0.91	1474
	NH_4^+	0.82	−0.10	0.86	1453
	Na^+	0.41	0.07	0.57	333
	K^+	0.56	0.02	0.41	151
	Mg^{2+}	0.73	0.06	0.59	109
	Ca^{2+}	2.83	−0.21	0.13	343
Midefix	NO_3^-	0.91	0.10	0.79	56
	SO_4^{2-}	0.70	0.66	0.71	56
	NH_4^+	0.64	0.05	0.68	26

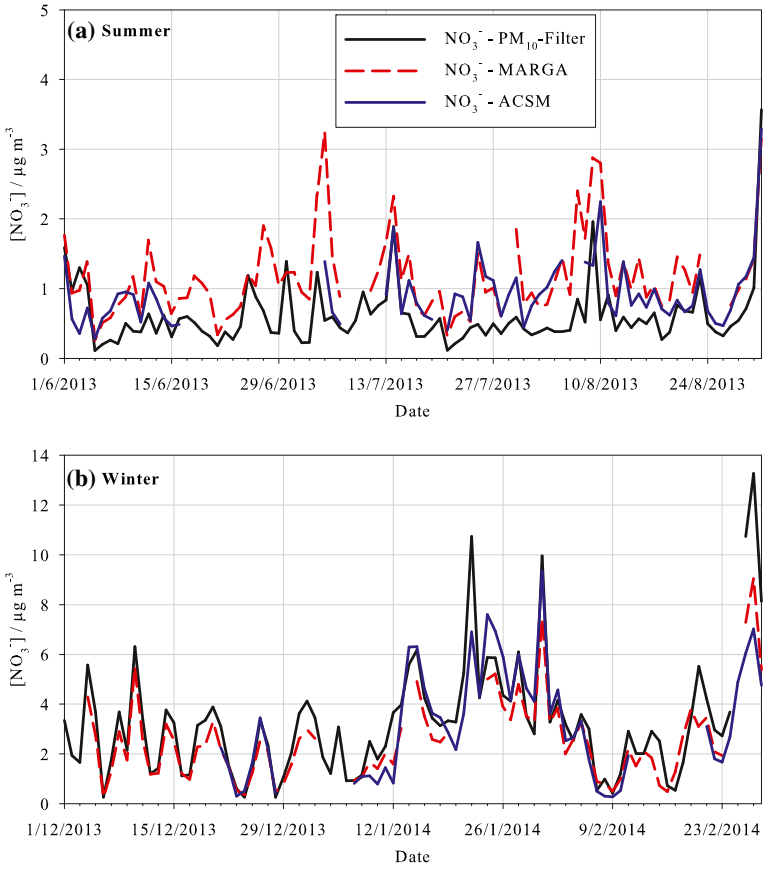

Fig. 8 Comparison of NO_3^- measured with MARGA (*red*). PM_{10} filter offline analysis (*black*), and ACSM (*blue*) during (**a**) summer 2013 and (**b**) winter 2013/14

for the comparison with the MARGA as for the PM_{10} filter cannot be detected. Possibly, the coating of the mini-filter suppresses the loss due to evaporation.

Rumsey et al. (2014) mentioned that a contamination with bacteria in the WRD and SJAC could lead to a depletion of NH_4^+. However, by means of the H_2O_2 used as biocide and regular cleaning of the WRD and SJAC at least every two weeks, a bacterial development could be avoided or strongly limited, and therefore this artifact may be minor. A microbiological depletion of NH_4^+ would result in an increase of NO_3^- (Rumsey et al. 2014), which has not been observed, neither in the latter nor in the present study.

The Midefix measurements for NH_4^+ and SO_4^{2-} concentrations show higher deviations and an underestimation compared to the MARGA. The Midefix detects more NH_4^+ than the measurements performed by the MARGA for the whole measurement period; this could be explained by the absorption of NH_3 on the filter surface, which had likely not been collected by the preceding coated denuder.

The concentrations of the non-NH_4^+ cations often remained below the detection limit. This results in a smaller number of compared points (*n*) by a factor of five to ten compared to the main ions (Table 5). Initial concentrations of magnesium (Mg^{2+}) and calcium (Ca^{2+}) show a

significant overestimation in 2010 and 2011. It emerged that over time both ions accumulate inside of the cation injection loop and can detach and spread again during later samples. Since 2012, the loops within the Melpitz MARGA have been renewed on a quarterly basis at the least. This issue is also described by Makkonen et al. (2012). Eventually, the years 2010 and 2011 were not used for comparison and further analysis.

Weak correlations for the non-NH_4^+ cations were found with an underestimation by the MARGA measurements, except for Ca^{2+}. A possible reason for the underestimation of the concentrations can be found in Thomas et al. (2009). The cited authors used the GRAEGOR system for the measurement of ions in the gas and particle phase and reported that 3.3% of PM_{10} are also detected within the WRD samples due to gravitational processes.

Nevertheless, the regressions for these ions in Makkonen et al. (2012) are comparable to those in this study. In the course of a subsequent study, the cation loop was replaced by a pre-concentration column, by means of which slopes near unity and better coefficients of determinations for potassium (K^+) and Na^+ could be observed. The measured concentrations of Ca^{2+} and Mg^{2+} were very low and led to weaker coefficients of determination but better slopes close to unity during their measurement period (Makkonen et al. 2014). The use of pre-concentration columns was not realized in Melpitz to avoid a change in the well-defined and complex analytical method used for this long-term study.

3.3 Results of the five-year measurement period

The hourly MARGA data allow us to investigate the daily cycle of the quantified concentrations in the gas and particle phase and their seasonal variations. As additional information, the maximum concentrations of each gaseous and particulate compound is given in the Electronic Supplementary Material in Table S1. The PSCF method visualizes the most probable geographical emission areas of each species. However, this method of calculation and modelling is more appropriate for the particle phase as the measured gases have shorter atmospheric lifetimes.

3.3.1 Gases

The measurement series for the trace gases as weekly averages and the diurnal variations for each season over the entire sampling period are plotted in Figs. 9 and 10, respectively.

The most distinct cycle for HNO_3 appears during the springtime (Fig. 10a). The highest springtime concentrations were measured during the time period from 10:00 AM to 4:00 PM CET. These concentrations are in agreement with the highest formation rate during daytime. Photolytically produced OH radicals react with nitrogen dioxide (NO_2) and form HNO_3 (Seinfeld and Pandis 2006; Griffith et al. 2015). This explains that the highest concentrations occur in summer as shown in Fig. 9. A possible photolysis of HNO_3 as a sink can be neglected in the troposphere since the photolysis is very slow (Möller 2003). The fast deposition onto surfaces and droplets is the main sink of HNO_3 (Ferm and Hellsten 2012), especially during nighttime. Another sink might be the nocturnal reaction of NO_3 radicals and alkanes. However, the rate constant is low and should be of minor importance (Seinfeld and Pandis 2006). In presence of NH_3, NH_4NO_3 can be formed depending on temperature and humidity (Möller 2003; Acker et al. 2006). As discussed in the previous section, the MARGA HNO_3 concentrations should be used critically because of its sticky behaviour.

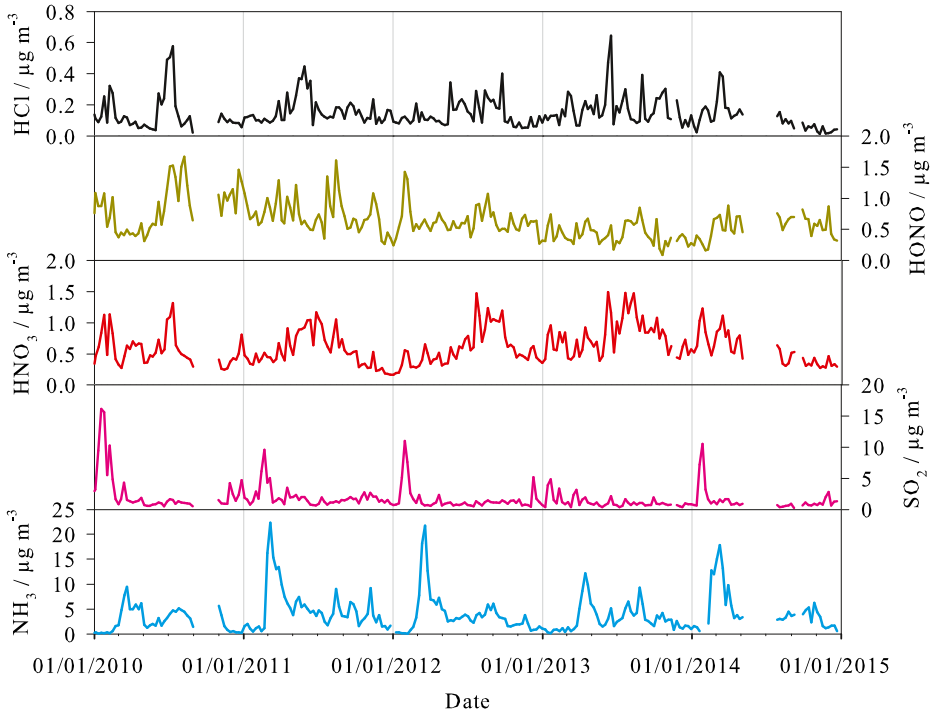

Fig. 9 Time courses of HCl (*black*), HONO (*olive*), HNO_3 (*red*), SO_2 (*pink*), and NH_3 (*blue*) as weekly averages from 2010 to 2014

Clear diurnal variations for HONO are observable, which are comparable to the ones reported by Pinto et al. (2014) and Acker et al. (2006), despite their known artifacts (see chapter 3.2.1). Figure 10b illustrates the HONO concentration differences between summertime and wintertime. Nighttime concentrations during the summer are on average twice as high as nighttime concentrations in winter. Possibly, the longer daylight hours in summer and more intense solar radiation favor the photolytic production of OH radicals. In the evening, in the presence of NO and absence of solar radiation, the radicals can react with HONO. In autumn and winter, the diurnal cycle is less pronounced than during spring and summer. At sunrise, the photolysis of HONO results in a decrease of measured concentrations. Beside possible positive artifacts caused by wet chemical sampling, HONO daytime sources also exist and explain low HONO concentrations despite of a strong photolysis. Several HONO daytime sources were discussed in literature (Li et al. 2014; Michoud et al. 2014; Spataro and Ianniello 2014; VandenBoer et al. 2014).

SO_2 as an anthropogenically emitted trace gas shows clear diurnal cycles in all seasons, as shown in Fig. 10c. Regarding the diurnal cycle of SO_2 for all seasons, the highest concentrations were measured in winter due to emissions by domestic heating and coal-fired power plants (Hamed et al. 2010) as well as enrichment in the inversion layer. Furthermore, for all seasons the highest concentrations occurred at noon, which is in agreement with the measurements performed by Henschel et al. (2013). The SO_2 noontime peak was investigated by Xu et al. (2014) for measurements performed in the North China Plain (NCP). The group tried to explain the peaks observed in the NCP with different reasons. For Melpitz, the most dominant enrichment processes of SO_2 probably lie in the transport into higher layers and down-mixing in the morning due to the break-up of the inversion layer by solar radiation.

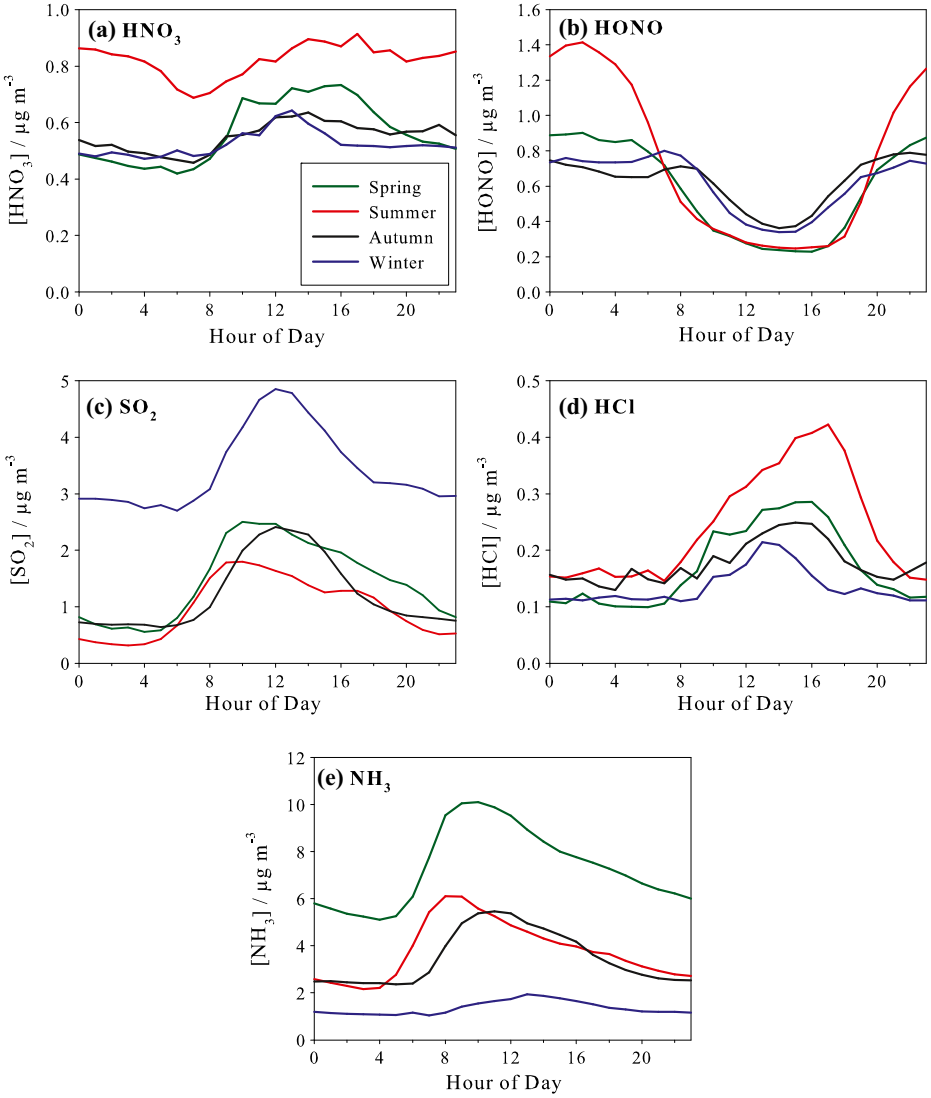

Fig. 10 Diurnal cycles of (**a**) HNO_3, (**b**) HONO, (**c**) SO_2, (**d**) HCl, and (**e**) NH_3 and their seasonal dependence for spring (*green*), summer (*red*), autumn (*black*), and winter (*blue*). Each average was calculated for the whole measurement period from 2010 to 2014

After reaching the noontime peak, the SO_2 concentration decreases during afternoon. This decline starts earlier during summer and spring than it does during autumn and winter. The atmospheric oxidation processes of SO_2 lead to a formation of gaseous sulfuric acid (H_2SO_4) or particulate SO_4^{2-} (Jones and Harrison 2011).

As SO_2 has a tropospheric lifetime of one week based on the rate constant for the reaction with OH radicals (Seinfeld and Pandis 2006), a long-range transport can occur effectively, making it possible to calculate the original emission area from which the SO_2 was transported to Melpitz. In Fig. 11, the PSCF analysis indicates South Poland, Czech Republic, Slovakia and possibly Austria as emitters of this trace gas that emerges mainly as a result of combustion

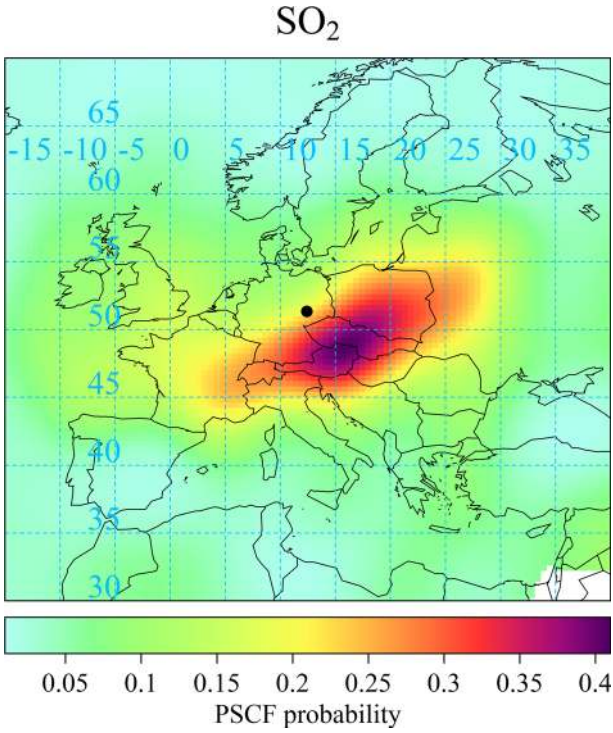

Fig. 11 PSCF analysis of SO_2 calculated using the open access R package 'Openair'. The colors correspond to the probability for the emission area as origin of the measured SO_2 in Melpitz (*black point*)

processes. In addition, the alpine regions as well as Eastern Poland seem to be likely emitters of SO_2 as well. However, the results of these PSCF plots are influenced by the respective form of the trajectories. For example, the air parcel over Eastern Poland is strongly polluted. Anticyclonic conditions force the air parcel to overflow Czech Republic and then approach Melpitz from a southeasterly direction. Further "polluted" trajectories from other directions can overflow Czech Republic in addition, leading to a high density of "polluted" trajectories. While the PSCF model maps the source potential of particular area it does not indicate the contribution of the source area to the measured concentrations (Hopke 2016).

As shown in Fig. 10d, the nocturnal concentrations of hydrochloric acid (HCl) range between 0.1 and 0.15 μg m^{-3} for all seasons, whereas the maximum daytime concentrations vary from 0.2 μg m^{-3} (in winter) to 0.4 μg m^{-3} (in summer), as a result of a higher radiation budget (see also Fig. 9). A shift in time between winter (12:00 AM, CET) and summer (4:00 PM, CET) was found for the observed maximum concentrations. The main contributions to the increase of HCl concentrations are to be found in surface reactions of H_2SO_4 and HNO_3 with sea salt aerosols (Pio and Lopes 1998; Seinfeld and Pandis 2006). Both acids reach their highest tropospheric concentrations after sunrise due to photochemical formations or meteorological influences. As SO_2 and HNO_3 reach their highest concentrations during daytime, it seems that their presence, SO_2 acting as a precursor of H_2SO_4, is essential to HCl formation in the afternoon. An additional HCl daytime source can be found in the evaporation of volatile particulate ammonium chloride (NH_4Cl) (Pio and Harrison 1987).

The lowest concentrations as well as the least distinct diurnal cycle for NH_3 can be found in winter (Fig. 10e). For the other seasons, a significant increase during the morning hours was observed, with averaged maximum concentrations of 10 μg m^{-3} detected during spring.

Figure 12 shows averaged NH_3 concentrations as a function of temperature, indicating a quick increase of NH_3 between 0 °C and 10 °C. This has several reasons: First, with increasing temperature, wet surfaces begin to evaporate dissolved NH_3 (Hesterberg et al. 1996). Second, with increasing temperature at the earth's surface, air masses become more labile, resulting in vertical mixing. Thus, volatile ammonium salts like NH_4Cl and NH_4NO_3 reach Melpitz through long-range transport and possibly mix into warmer near surface air masses, where the salts evaporate to NH_3, HNO_3 and HCl. These higher NH_3 concentrations during the early morning hours, caused by turbulent transport, often occurred simultaneously with an increase in SO_2. The third reason can be found in the end of the legal blocking period (1st of March) for liquid manure fertilization in the surroundings of the TROPOS research station in Melpitz. Fertilization is not allowed as long as the soil is still frozen or saturated with water. Only at positive temperatures and when dry soil surfaces are given, liquid manure may be used. The latter also explains the high concentrations observed during spring (Ferm and Hellsten 2012). The last possibility that has to be taken into account when considering the peak in the morning is a possible memory effect of the inlet system (see chapter 3.2.1). Increasing temperatures in the morning could then lead to an evaporation of deposited NH_3 within the inlet.

3.3.2 Particulate ions

Figure 15a shows two important sources of Cl^- occurring in different temperature intervals. At below −8 °C, the averaged Cl^- concentrations vary between 0.4 and 0.6 μg m^{-3}A second maximum of the Cl^- concentrations with 0.5 μg m^{-3} exists at temperatures slightly above zero. Both maxima have individual sources. In addition, the diurnal variability for the different seasons is shown in Fig. 16a.

For temperatures <−8 °C, the sampled aerosol can consist of Cl^- originating from the combustion of Cl^--containing coal in Eastern Europe (Xie et al. 1997; McCulloch et al. 1999; Spindler et al. 2013; Tang et al. 2015). Consistently, at very cold temperatures, the

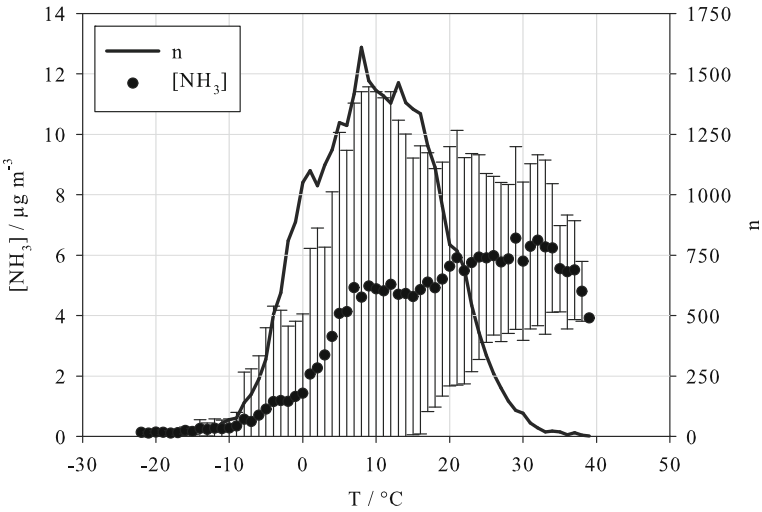

Fig. 12 Influence of the temperature on the NH_3 concentration. The points indicate the averaged concentrations per degree with the standard deviation as error bars. The number of data points *n* considered for averaging is displayed as the line plot (*right ordinate*)

predominant air mass inflow is coming from an easterly direction, as shown in Fig. 15b. The figure shows the frequency of a respectively observed wind direction as a function of Cl^- occurrence. In winter, an additional local contribution to the higher Cl^- concentrations lies in the reemission of road salt used for the de-icing of streets. When observing measured Cl^- in relation to wind direction and wind speed (Figs. 15c,d), the highest averaged concentrations can be detected at northeasterly and southwesterly winds. Relative to Melpitz, there are two main roads situated in this direction that are gritted with salt in winter. However, influences originating from the cities of Torgau and Leipzig, which are also located in these directions, can also contribute to the amount of Cl^- measured in Melpitz. These findings are in agreement with Fig. 16a, showing high Cl^- concentrations (0.4 μg m^{-3}) during winter.

The second maximum is observed at moderate temperatures (Fig. 15a) and can be explained by the sum of two effects. Firstly, similarly to NH_3 (see section 3.1.1), the Cl^- concentrations are high at temperatures over 0 °C. This parallel increase leads to the conclusion that, again, the agricultural use of Cl^- (artificial fertilizer) explains its high concentrations in spring (Fig. 16a). Secondly, the increase of Cl^- at moderate temperatures indicates more marine influences. Sea salt aerosol originating from long-range transport consists mainly of Cl^- that is measured in Melpitz. The highest wind speeds measured in Melpitz occurred mainly during autumn and winter and from westerly directions, which explains the dominant Cl^- peak at moderate temperatures.

The lowest Cl^- concentrations occurred in summer, with 0.2 μg m^{-3}. Pio and Lopes (1998) found that, especially in summer, a loss of Cl^- within the particulate matter due to volatilization can be observed. The degassing of chlorine takes place through reactions with acidic sulphur compounds for fine particles and HNO_3 for the course mode.

The PSCF analysis for the five-year measurement period highlighted the marine origin of Cl^- as well as its emission from coal combustion. Figure 17a clearly indicates marine air masses from the North Sea as one of the main contributors to the analyzed Cl^- concentrations in Melpitz. A second emission area covers a large area including Austria, Czech Republic, Poland and Slovakia that contributes to anthropogenic emissions. Thereby, the shift in the respective contribution factors is clearly identifiable for the different seasons (Fig. 18). In spring, the dominant source of Cl^- can be found in marine aerosols; anthropogenic aerosols from the east however only give minor contributions. In summer, only the presence of sea salt adds to the measured concentrations in Melpitz. Contribution by the eastern component starts to increase again in autumn and grows to be the major contributor in winter.

The diurnal cycles of NO_3^- (Fig. 16b) and NH_4^+ (Fig. 16c) show their highest values in the morning, caused by the start of vertical mixing, and a decrease in the afternoon. This course in time is equally pronounced during every season. In the fine mode, NO_3^- is mainly bound in the form of NH_4NO_3, which is dependent on the gas phase precursor concentrations, temperature, humidity, and aerosol chemical composition (Poulain et al. 2011; Twigg et al. 2015). The volatile behaviour of NH_4NO_3 results in the formation of the gaseous compounds HNO_3 and NH_3 for higher temperatures and low humidity. In winter, NH_4NO_3 exists predominantly in the particle phase (Seinfeld and Pandis 2006), explaining higher concentrations for NO_3^- and NH_4^+ (Fig. 16b,c). High values of NO_3^- and NH_4^+ in spring are attributed to agricultural fertilization.

In winter, SO_4^{2-} reaches its highest concentrations but shows no diurnal variation (Fig. 16d). The anthropogenic SO_4^{2-} is emitted from domestic heating processes and can, additionally, be enriched in the atmospheric boundary layer. Similar results were reported by Spindler et al. (1999) and Cyrys et al. (1995). A slight increase of the SO_4^{2-} concentration at noon and during the afternoon is recognizable for the other seasons. This is in good agreement

with the findings in the prior chapter. The formation of SO_4^{2-} as a result of atmospheric oxidation processes of SO_2 can explain this peak during daytime.

A relationship between the measured NO_3^-, SO_4^{2-} and NH_4^+ can be determined through the calculation of the most probable emission areas. Exhibiting red and violet colors in Fig. 17b-d, and nearly the same spatial extent, all three ions show high concentrations when air mass transport from easterly directions is given. Similar to SO_2 and anthropogenic Cl^-, the highest probabilities with over 50%, 30% and 40% for SO_4^{2-}, NO_3^- and NH_4^+, respectively, were calculated for areas stretching over the Czech Republic, Slovakia and Southern Poland. Moreover, all of these compounds show their highest concentrations in the winter months (Figs. 9 and 13). Thermo-stable ammonium sulphate shows the lowest vapor pressure of all ammonium salts and is the first to form (Ferm 1998). In addition, the thermo-volatile NH_4NO_3 exists in the particle phase in winter. These salts can reach Melpitz through long-range transport. Additionally, fine mode NO_3^- is formed during the oxidation of NO_x emissions of anthropogenic origin, while the chloride-nitrate exchange leads to the formation of course mode NO_3^- particles, even over Central and Western Europe (Dasgupta et al. 2007; Twigg et al. 2015). This can explain the high emission probability shown in Fig. 17b. Ferm and Hellsten (2012) measured particulate ion concentrations in several sites in Sweden and observed an inflow of high NO_3^-, NH_4^+ and SO_4^{2-} concentrations in particles transported from the south. These ions were transported in the solid phase over long distances from Central Europe, since these particles have a lower deposition velocity than their gaseous precursors in Central Europe. In Ferm (1998), the averaged NH_4^+ concentrations of several European sites were shown for different wind sectors. Thereby, the western and central European sites all

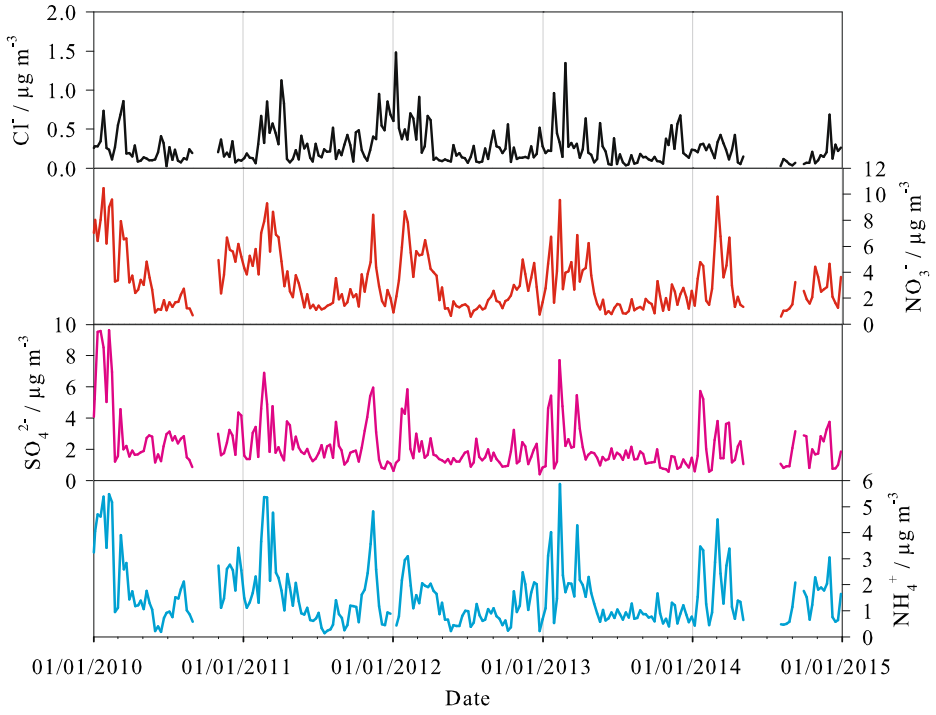

Fig. 13 Time courses of Cl^- (*black*), NO_3^- (*red*), SO_4^{2-} (*pink*), and NH_4^+ (*blue*) as weekly averages from 2010 to 2014

indicate an easterly origin of NH_4^+. The results of both studies agree with the air mass origin of NH_4^+ found in the present study.

The number of detected non-NH_4^+ cations is lower in comparison to the main ions (see chapter 3.1). A clear diurnal cycle for K^+ cannot be recognized in Fig. 16e, but in winter, higher concentrations could be observed at midnight and the following hours. However, these high mean values during nighttime are primarily the result of only three days in the five-year long-time period that showed high K^+ concentrations. On New Year's Eve, fireworks emit large amounts of potassium nitrate into the troposphere. This could be observed for the years 2010, 2011 and 2014. During these days in 2012 and 2013, the MARGA in Melpitz was out of service. The impact of fireworks on the atmospheric pollution was also investigated by means of the MARGA by Wen and Chen (2013). Therein, the K^+ concentration was used as a tracer for firework events. Generally, higher K^+ concentrations were observed during the winter months. The main K^+ source is thereby wood combustion. The PSCF calculation for K^+ (Fig. 17e) ascribed the main emission areas to regions situated to the east of Melpitz and the Alps, which indicates an anthropogenic source, as domestic heating with wood is more common in these regions.

For the sea salt tracers Na^+ and Mg^{2+} (Perrino et al. 2010), a marine origin becomes obvious in Fig. 17f, g. Both are transported to the measurement site in form of NaCl and magnesium chloride ($MgCl_2$), or processed as $NaNO_3$, with westerly winds. Correspondingly, the calculated maps of their emission areas show their highest concentrations above the North Sea and the northern Atlantic Ocean. This is in good agreement with analysis made for Cl^-. (Fig. 17a). Additionally, high Mg^{2+} concentrations in winter (Fig. 16f) could be attributed to the de-icing of streets using road salt, acting as a source in the surroundings.

Very high concentrations of Ca^{2+} were observed in spring. In comparison to the detected Ca^{2+} concentrations in spring, as shown in Fig. 16g, the concentrations measured in other seasons were lower by a factor of 2.5. As both Mg^{2+} and Ca^{2+} show high concentrations in spring, a related effect could be possible. These high values were detected in spring 2012 (Fig. 14). The possibility that high concentrations occurred due to the formation of artifacts within the sample loop can be neglected as they have been exchanged periodically since 2012. Another possible reason could be the application of mineral fertilizer in agriculture and forestry in 2012.

Further sources of particulate Ca^{2+} can be found in the re-emission of calcium carbonate and calcium sulphate as well as the reactions of HNO_3 and H_2SO_4 with mineral dust particles (Metzger et al. 2006), which could account for part of the high spring concentrations.

3.3.3 Particulate acidity

In the literature, different estimations on particulate acidity were found. The most used calculation method is the Molar Ratio (MR) for the measured ions (Eq. 2). Since NH_4^+, SO_4^{2-} and NO_3^- are the dominant acidifying compounds in the particulate phase, the MR is often simplified for these major inorganic compounds. This simplified ratio is called Neutralisation Ratio (NR) (Eq. 3). Ions are expressed as equivalents.

$$MR = \frac{\sum \text{cations}}{\sum \text{anions}} \tag{2}$$

$$NR = \frac{\left[NH_4^+\right]}{\left[NO_3^-\right] + 2\left[SO_4^{2-}\right]} \tag{3}$$

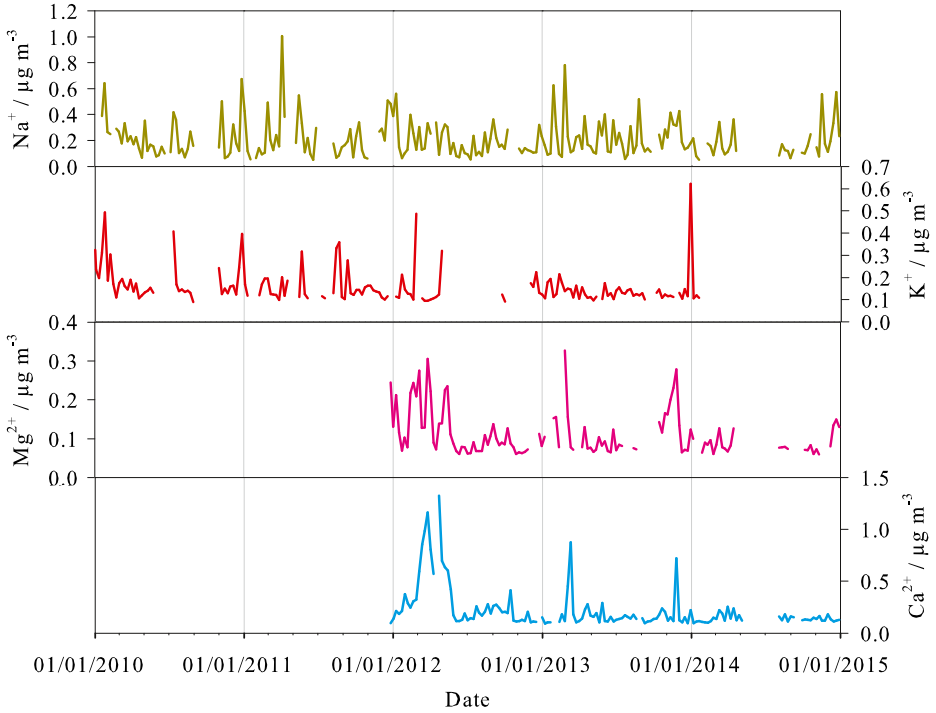

Fig. 14 Time courses of Na^+ (*olive*), K^+ (*red*), Mg^{2+} (*pink*), and Ca^{2+} (*blue*) as weekly averages from 2010 to 2014

Recently, Hennigan et al. (2015) evaluated proxy methods to estimate aerosol pH and concluded that the calculation using the MR is not recommendable as it neglects aerosol water as well as partial dissolution of acids and ions on pH; also, there are limitations, resulting from analytical issues. Nevertheless, as these calculations are common in the analysis of particle measurements, this still poses a possibility to compare the ratios at different sites.

For Melpitz, the calculations using the MRs and NRs for the five-year measurement period amount to 0.90 and 0.79, respectively, which implies that the measurement site is predominantly influenced by slightly acidic particles. The lowest cation-to-anion-ratios occurred during autumn and winter. This is probably due to anthropogenic emissions. As for the years 2010 and 2011, the concentrations of Mg^{2+} and Ca^{2+} could not be considered due to sampling artifacts. The averaged MR and NR were recalculated for the years 2012 to 2014 and reach 1.0 and 0.82, respectively. A MR of 1.0 is an indicator for neutral conditions. However, the slightly higher NR that is not dependent on both cations still indicates slight acidic conditions for the last three measurement years. Figure 19 shows the calculated NRs and the averaged equivalent concentrations of the sum of NH_4^+ and Na^+ concentration values as well as the sum of Cl^-, NO_3^- and SO_4^{2-} concentration values for every season from 2010 to 2014. The seasonal variations of the ions, with high concentrations in winter and lower concentrations in summer, are clearly visible. During the measurement period, a decreasing trend for the ions can be observed for Melpitz, which is in agreement with a slightly decreasing particle mass concentration detected by high-volume filter measurements (PM_{10}). However, a clear seasonal dependence of the NR cannot be identified. The NR strongly fluctuates between 0.5 and 1. Acidic particles were dominant in summer of 2011 and winter of 2012. In winter 2012, marine

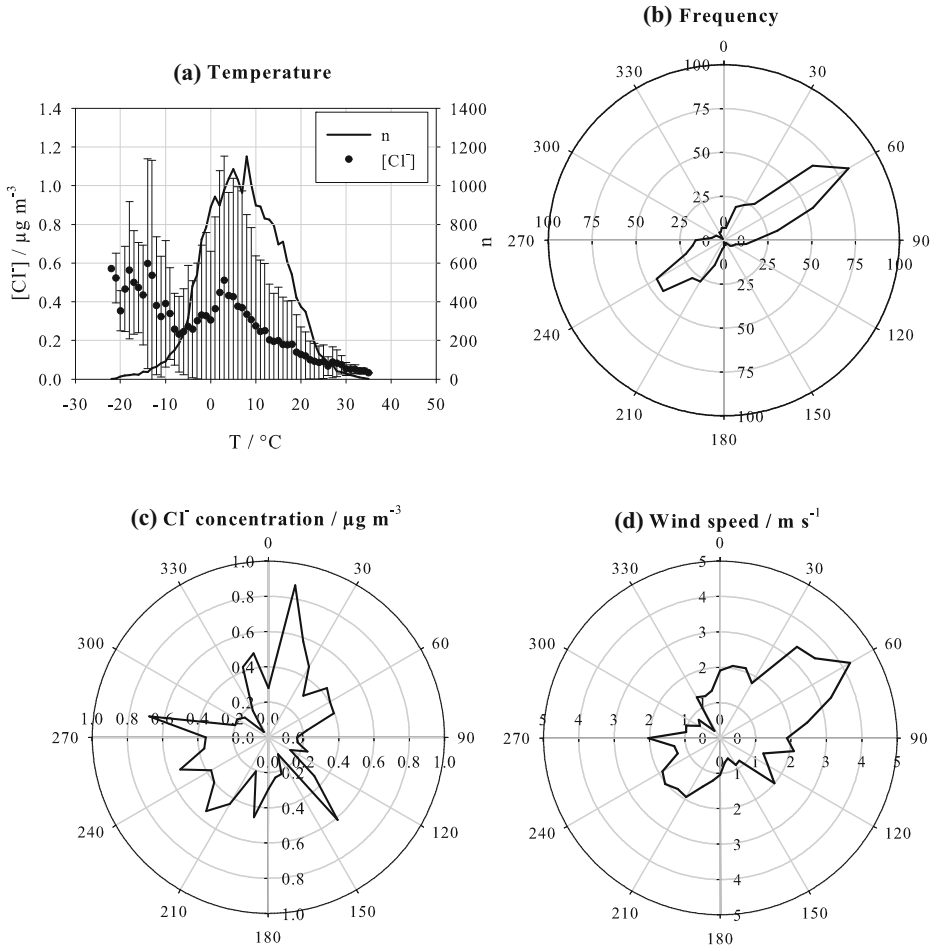

Fig. 15 (**a**) Influence of temperature on Cl^- concentration. The points represent the averaged concentrations per degree with the standard deviation as error bars. The number of data points *n* considered for averaging is displayed as the line plot (*right ordinate*). (**b**) Wind dependence on the frequency, (**c**) Cl^- concentration, and (**d**) wind speed for the temperature interval of <−8 °C in Melpitz during the measurement period

aerosols were significant. The additional calculation of the cation-to-anion ratio with Na^+ and Cl^- and the other main ions of the NR for the measurement period (in Fig. 19 described as NR with sea salt) lead to an increase in the ratio of approximately 0.1 for nearly all seasons. However, for winter 2012, the increase was around 0.3, indicating a marine influence. The reason for the low peak in summer 2011 remains unclear, although, dust, possibly, could have been an influencing factor. As there are no data for Ca^{2+}, this assumption cannot be verified for this period. After 2012, the ratio increased and then remained the same level, which led to the higher NR in the following three years (on average 0.82). A stronger decrease of NO_3^- and SO_4^{2-} in comparison to NH_4^+ might explain the increase of NR.

Makkonen et al. (2012) observed predominantly acidic particles in winter and basic aerosol in spring due to road dust emissions, resulting in high Ca^{2+} concentrations, in Finland. Recently, Twigg et al. (2015) investigated particle acidity in Auchencorth Moss in southeast Scotland and found mostly an excess of NH_4^+. Closer to Melpitz, Ferm and Hellsten (2012)

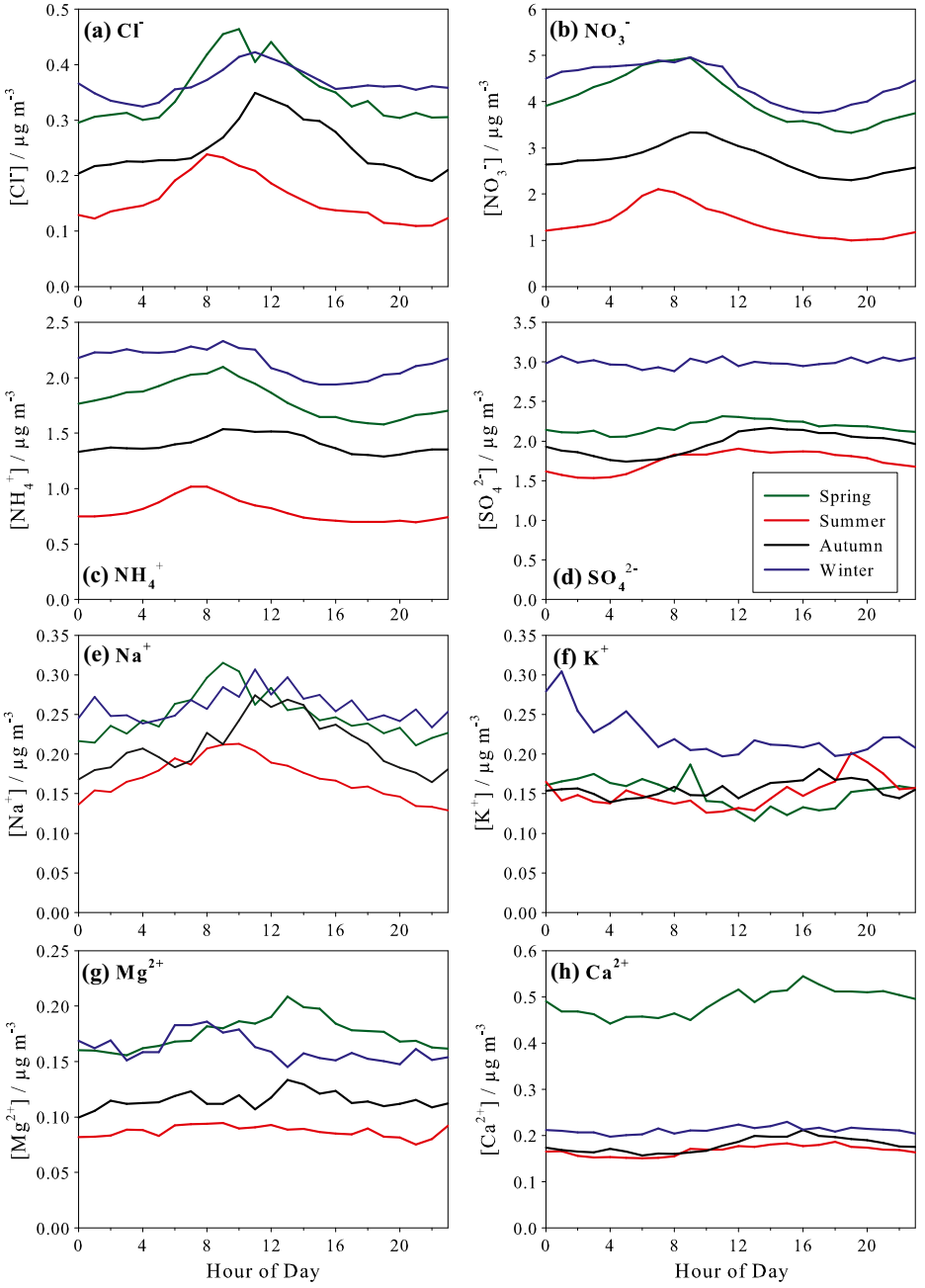

Fig. 16 Diurnal cycles of (**a**) Cl^-, (**b**) NO_3^-, (**c**) NH_4^+, (**d**) SO_4^{2-}, (**e**) Na^+, (**f**) K^+, (**g**) Mg^{2+}, and (**h**) Ca^{2+} and their seasonal dependence for spring (*green*), summer (*red*), autumn (*black*), and winter (*blue*). Each average was calculated for the whole measurement period from 2010 to 2014

determined and compared the annual average of NH_4^+ as well as the anions NO_3^- and SO_4^{2-} in Vavihill, situated in Southern Sweden. At this site, the anions dominated over a

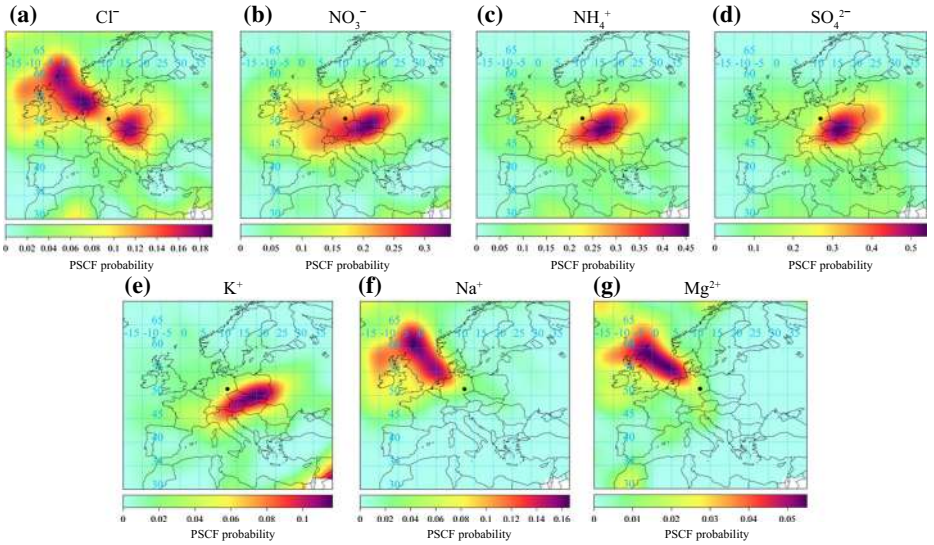

Fig. 17 PSCF analysis of (**a**) Cl^-, (**b**) NO_3^-, (**c**) NH_4^+, (**d**) SO_4^{2-}, (**e**) K^+, (**f**) Na^+ and (**g**) Mg^{2+} over five years calculated using the open access R package 'Openair'. The colors correspond to the probability that the respective region is the most likely emission area of the measured particulate ions in Melpitz (*black point*)

measurement period of 18 years. These authors demonstrated that high NH_4^+ concentrations correlate with air-mass transport from the south. Thus, other anthropogenically emitted ions such as SO_4^{2-} and NO_3^- could have been transported to Vavihill from Central Europe, resulting in more acidic particles. Squizzato et al. (2013) measured the particulate composition at three sites around Venice, Italy, and subsequently determined the NR. Except for during winter periods, ratios ranged from 0.7 to 0.9. At two sites, the ratio exceeded 1.1, indicating an excess of NH_4^+. Measurements during the summer of 2003 in K-puszta, Hungary, showed both fine and coarse mode MRs of 1.25 and 2.87, respectively (Ocskay et al. 2006). The PSCF analysis in chapter 3.3.2 of the present paper indicates high emissions of anthropogenic particulate ions near Hungary that are more acidic. Nevertheless, the particles are strongly basic. Probably, mineral dust particles are the major contributor to the calculated ratio for the coarse mode in K-puszta.

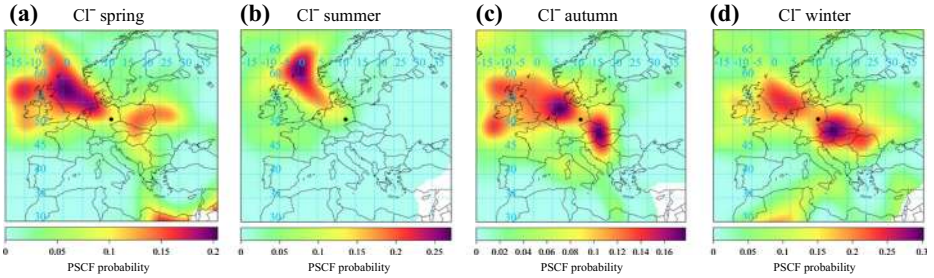

Fig. 18 PSCF analysis of Cl^- in (**a**) spring, (**b**) summer, (**c**) autumn, and (**d**) winter over five years calculated using the open access R package 'Openair'. The colors correspond to the probability that the respective reason is the most likely emission area of the measured particulate ions in Melpitz (*black point*)

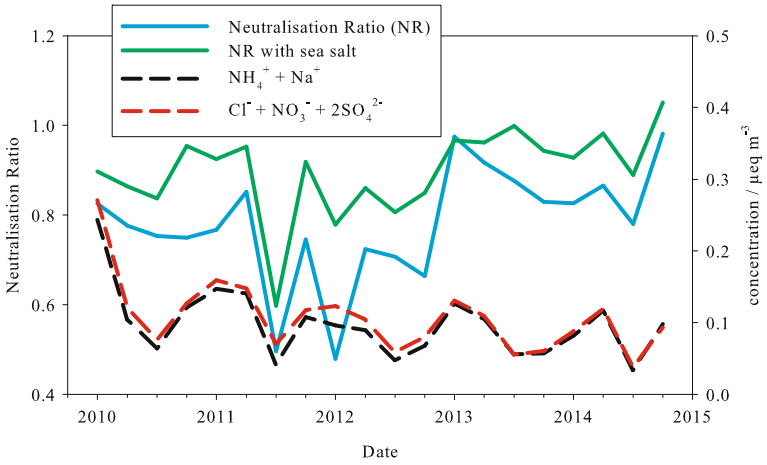

Fig. 19 Seasonally averaged Neutralisation Ratio (NR) (*blue, solid*), NR with sea salt (NaCl) (*green, solid*), the sum of $NH_4^+ + Na^+$ as equivalent concentration (*black, dashed*), and the sum of $Cl^- + NO_3^- + 2SO_4^{2-}$ (*red, dashed*) as equivalent received from MARGA data from 2010 to 2014

4 Conclusions

Results of concentration measurements for gases and ions in PM_{10} using MARGA in Melpitz were presented from 2010 to 2014. Besides an evaluation of the instruments, the received data were used to explain diurnal gas concentrations as well as to characterize PM_{10} with a high time resolution at Melpitz over the whole measurement period.

During this time, different comparisons were executed in order to validate the MARGA system. It was found that some gases are difficult to quantify. A direct comparison to another denuder system without inlet bared great discrepancies for the HNO_3 analysis. Its "sticky" behaviour coupled with the influence of the MARGA inlet system results in a strong underestimation. For HONO, the comparison between the denuder and the MARGA shows a slope near unity but a large scatter field with a weak coefficient of determination of 0.41. The difference between both denuder based sampling methods occurs possibly due to different inlet systems, offline analysis for the batch denuder samples and the impact of heterogeneous reactions within the denuders. Also for the MARGA measurements of NH_3, possible artifacts should be considered. Similar to HNO_3, NH_3 has a high potential to adsorb onto the walls. Thus, possible memory effects due to the inlet system could influence the measured concentrations. However, the comparison with different coated denuders showed on average higher concentrations for the MARGA system. The duration time of the gases within the coated denuders was probably too short. However, good correlations of 0.91 and 0.73 and slopes near unity were achieved for the SO_2 comparison with a SO_2 gas monitor and a Midefix, respectively.

Despite of different cut-off diameters, good agreements were observed for the particulate SO_4^{2-} and NH_4^+ for the comparisons of MARGA with the ACSM with slopes of 1.39 and 1.20, respectively. Organic nitrates that can be measured by the ACSM could possibly explain the slope of 0.88 for NO_3^-. An important advantage of the MARGA is the sampling of the particles free of evaporation artifacts. Accumulated particles in the filter can often interact with ambient gases depending on meteorological conditions. Possible losses due to evaporation of semivolatile particles or positive artifacts due to the adsorption of gases in the filter cannot be

excluded for filter measurements. However, the MARGA sampling is also limited by the high time resolution of one hour. The hourly concentrations of Na^+, K^+, Mg^{2+} and Ca^{2+} in ambient air are low, as the liquid concentrations of these ions within the MARGA often did not exceed the detection limit and could not be quantified.

Long-term measurements in Melpitz allow us to investigate the variations in time for different compounds. Except for HONO, the gas concentrations peak during daytime. For HCl, photolytic production explains high concentrations in the afternoon and in summertime. The measured noontime peaks of SO_2 for all seasons in Melpitz can be explained by transport and down-mixing after the formation of the planetary boundary layer. High concentrations in winter occur due to elevated emissions from domestic heating and an additional enrichment caused by the formation of an inversion layer. NH_3 concentrations increase strongly after sunrise. Increasing temperatures lead to an evaporation of both dew droplets in which the gas was dissolved and semi-volatile NH_4NO_3 in particles that can be transported over a longer range. The well pronounced diurnal cycle of HONO with low concentrations during daytime indicates that despite of a strong photodissociation, additionally, a significant photochemical daytime source exists. Besides, possible heterogeneous reactions within the MARGA denuder could result in an offset of the measured HONO concentrations.

While the gases have mainly local sources, the PSCF analysis and wind data indicate transport processes as the major contributor to the measured particulate concentrations. Thereby, marine and anthropogenic sources could be distinguished. Coarse mode Cl^-, Na^+ and Mg^{2+} are the major compounds of sea salt. Both the PSCF analysis and the wind data indicate an origin lying in westerly directions, specifically over the North Sea and the Atlantic Ocean. However, the major contributions to inorganic PM_{10} are NO_3^-, SO_4^{2-} and NH_4^+. The highest concentrations were found in winter at easterly winds. The PSCF analysis calculated the most probable area for anthropogenic emissions over Southern Poland, Czech Republic and Slovakia, from where the particulate ions are transported to the Melpitz site. In addition, Cl^- and K^+ in fine particles also seem to have their origin in this area. They are important indicators of anthropogenic combustion processes.

In order to estimate the acidity of the particles, the MR and NR were calculated. Calculated over the whole measurement period, the MR is 0.9. As the concentrations of Mg^{2+} and Ca^{2+} are not available for 2010 and 2011 as a result of analytical artifacts, the MR was calculated for the years 2012 to 2014. With a MR of 1.0, the particles were on average neutral. However, the NR indicates that the sum of NO_3^- and SO_4^{2-} seems to decrease faster than NH_4^+ so that the above mentioned three years were less acidic than the years 2010 and 2011.

Acknowledgements The authors acknowledge financial support of this study and deployment of the MARGA system by the German Federal Environment Agency (UBA) research foundation under contracts No: 351 01 093 and 351 01 070, as well as the European Union within the projects EUSAAR (European Supersites for Atmospheric Aerosol Research) under contract No: RII3-CT-2006-026140, ACTRIS and ACTRIS-2 (Aerosol, Clouds, and Trace gases Research InfraStructure Network) under grant agreements No 262254 and 654109 (Horizon 2020), respectively.

For the laboratory analysis and the preparation of filters and solutions, we thank A. Dietze, A. Rödger and S. Fuchs. For the support especially in the field, we thank R. Rabe.

References

Acker, K., Febo, A., Trick, S., Perrino, C., Bruno, P., Wiesen, P., Möller, D., Wieprecht, W., Auel, R., Giusto, M., Geyer, A., Platt, U., Allegrini, I.: Nitrous acid in the urban area of Rome. Atmos Environ. **40**(17), 3123–3133 (2006). doi:10.1016/j.atmosenv.2006.01.028

Acker, K., Spindler, G., Brüggemann, E.: Nitrous and nitric acid measurements during the INTERCOMP2000 campaign in Melpitz. Atmos Environ. **38**(38), 6497–6505 (2004). doi:10.1016/j.atmosenv.2004.08.030

Allen, H.M., Draper, D.C., Ayres, B.R., Ault, A.P., Bondy, A.L., Takahama, S., Modini, R.L., Baumann, K., Edgerton, E., Knote, C., Laskin, A., Wang, B., Fry, J.L.: Influence of crustal dust and sea spray supermicron particle concentrations and acidity on inorganic NO_3^- aerosol during the 2013 Southern oxidant and aerosol study. Atmos Chem Phys. **15**(18), 10669–10685 (2015). doi:10.5194/acp-15-10669-2015

Behera, S.N., Betha, R., Balasubramanian, R.: Insights into chemical coupling among acidic gases, ammonia and secondary inorganic aerosols. Aerosol Air Qual Res. **13**(4), 1282–U1414 (2013). doi:10.4209/aaqr.2012.11.0328

Berden, G., Peeters, R., Meijer, G.: Cavity ring-down spectroscopy: experimental schemes and applications. Int Rev Phys Chem. **19**(4), 565–607 (2000). doi:10.1080/014423500750040627

Canagaratna, M.R., Jayne, J.T., Jimenez, J.L., Allan, J.D., Alfarra, M.R., Zhang, Q., Onasch, T.B., Drewnick, F., Coe, H., Middlebrook, A., Delia, A., Williams, L.R., Trimborn, A.M., Northway, M.J., DeCarlo, P.F., Kolb, C.E., Davidovits, P., Worsnop, D.R.: Chemical and microphysical characterization of ambient aerosols with the aerodyne aerosol mass spectrometer. Mass Spectrom Rev. **26**(2), 185–222 (2007). doi:10.1002/mas.20115

Carslaw, D.C., Ropkins, K.: openair - An R package for air quality data analysis. Environ Model Softw. **27-28**, 52–61 (2012). doi:10.1016/j.envsoft.2011.09.008

Chen, H.Z., Wu, D., Yu, J.Z.: Comparison of characteristics of aerosol during rainy weather and cold air-dust weather in Guangzhou in late March 2012. Theor Appl Climatol. **124**(1–2), 451–459 (2016). doi:10.1007/s00704-015-1424-z

Chow, J.C., Lowenthal, D.H., Chen, L.W.A., Wang, X.L., Watson, J.G.: Mass reconstruction methods for $PM_{2.5}$: a review. Air Qual Atmos Hlth. **8**(3), 243–263 (2015). doi:10.1007/s11869-015-0338-3

Cyrys, J., Gutschmidt, K., Brauer, M., Dumyahn, T., Heinrich, J., Spengler, J.D., Wichmann, H.E.: Determination of acidic sulfate aerosols in urban atmospheres in Erfurt (F.R.G.) and Sokolov (former C.S.S.R.) Atmos Environ. **29**(23), 3545–3557 (1995). doi:10.1016/1352-2310(95)00133-J

Dämmgen, U., Thöni, L., Lumpp, R., Gilke, K., Seitler, E., Bullinger, M.: Feldexperiment zum Methodenvergleich von Ammoniak- und Ammonium-Konzentrationsmessungen in der Umgebungsluft 2005 bis 2008 in Braunschweig. vTI Agriculture and Forestry Research - Sonderheft. **337**, 62 (2010a)

Dämmgen, U., Thöni, L., Lumpp, R., Gilke, K., Seitler, E., Bullinger, M.: Verfahrenskenngrößen für die Bestimmung von Ammoniakkonzentrationen in der Umgebungsluft - Teil 1: Messungen mit Denudern. Gefahrst Reinhalt L. **5/2010**, 197–201 (2010b)

Dasgupta, P.K., Campbell, S.W., Al-Horr, R.S., Ullah, S.M.R., Li, J.Z., Amalfitano, C., Poor, N.D.: Conversion of sea salt aerosol to $NaNO_3$ and the production of HCl: analysis of temporal behavior of aerosol chloride/nitrate and gaseous HCl/HNO_3 concentrations with AIM. Atmos Environ. **41**(20), 4242–4257 (2007). doi:10.1016/j.atmosenv.2006.09.054

Du, H.H., Kong, L.D., Cheng, T.T., Chen, J.M., Du, J.F., Li, L., Xia, X.G., Leng, C.P., Huang, G.H.: Insights into summertime haze pollution events over Shanghai based on online water-soluble ionic composition of aerosols. Atmos Environ. **45**(29), 5131–5137 (2011). doi:10.1016/j.atmosenv.2011.06.027

Du, H.H., Kong, L.D., Cheng, T.T., Chen, J.M., Yang, X., Zhang, R.Y., Han, Z.W., Yan, Z., Ma, Y.L.: Insights into ammonium particle-to-gas conversion: non-sulfate ammonium coupling with nitrate and chloride. Aerosol Air Qual Res. **10**(6), 589–595 (2010). doi:10.4209/aaqr.2010.04.0034

Ellis, R.A., Murphy, J.G., Markovic, M.Z., VandenBoer, T.C., Makar, P.A., Brook, J., Mihele, C.: The influence of gas-particle partitioning and surface-atmosphere exchange on ammonia during BAQS-met. Atmos Chem Phys. **11**(1), 133–145 (2011). doi:10.5194/acp-11-133-2011

Fan, J., Yue, X.Y., Jing, Y., Chen, Q., Wang, S.G.: Online monitoring of water-soluble ionic composition of PM_{10} during early summer over Lanzhou City. J Environ Sci-China. **26**(2), 353–361 (2014). doi:10.1016/S1001-0742(13)60431-3

Ferm, M.: Atmospheric ammonia and ammonium transport in Europe and critical loads: a review. Nutr Cycl Agroecosyst. **51**(1), 5–17 (1998). doi:10.1023/A:1009780030477

Ferm, M., Hellsten, S.: Trends in atmospheric ammonia and particulate ammonium concentrations in Sweden and its causes. Atmos Environ. **61**, 30–39 (2012). doi:10.1016/j.atmosenv.2012.07.010

Finlayson-Pitts, B.J., Pitts, J.N.: Atmospheric chemistry: fundamentals and experimental techniques. John Wiley & Sons, Inc., New York (1986)

Fu, H., Zhang, M., Li, W., Chen, J., Wang, L., Quan, X., Wang, W.: Morphology, composition and mixing state of individual carbonaceous aerosol in urban Shanghai. Atmos Chem Phys. **12**(2), 693–707 (2012). doi:10.5194/acp-12-693-2012

Genfa, Z., Slanina, S., Boring, C.B., Jongejan, P.A.C., Dasgupta, P.K.: Continuous wet denuder measurements of atmospheric nitric and nitrous acids during the 1999 Atlanta supersite. Atmos Environ. **37**(9–10), 1351–1364 (2003). doi:10.1016/S1352-2310(02)01011-7

Griffith, S.M., Huang, X.H.H., Louie, P.K.K., Yu, J.Z.: Characterizing the thermodynamic and chemical composition factors controlling $PM_{2.5}$ nitrate: Insights gained from two years of online measurements in Hong Kong. Atmos Environ. **122**, 864–875 (2015). doi:10.1016/j.atmosenv.2015.02.009

Hamed, A., Birmili, W., Joutsensaari, J., Mikkonen, S., Asmi, A., Wehner, B., Spindler, G., Jaatinen, A., Wiedensohler, A., Korhonen, H., Lehtinen, K.E.J., Laaksonen, A.: Changes in the production rate of secondary aerosol particles in Central Europe in view of decreasing SO_2 emissions between 1996 and 2006. Atmos Chem Phys. **10**(3), 1071–1091 (2010)

Hennigan, C.J., Izumi, J., Sullivan, A.P., Weber, R.J., Nenes, A.: A critical evaluation of proxy methods used to estimate the acidity of atmospheric particles. Atmos Chem Phys. **15**(5), 2775–2790 (2015). doi:10.5194/acp-15-2775-2015

Henschel, S., Querol, X., Atkinson, R., Pandolfi, M., Zeka, A., Le Tertre, A., Analitis, A., Katsouyanni, K., Chanel, O., Pascal, M., Bouland, C., Haluzai, D., Medina, S., Goodman, P.G.: Ambient air SO_2 patterns in 6 European cities. Atmos Environ. **79**, 236–247 (2013). doi:10.1016/j.atmosenv.2013.06.008

Herrmann, H.: Kinetics of aqueous phase reactions relevant for atmospheric chemistry. Chem Rev. **103**(12), 4691–4716 (2003). doi:10.1021/cr020658q

Herrmann, H., Brüggemann, E., Franck, U., Gnauk, T., Löschau, G., Müller, K., Plewka, A., Spindler, G.: A source study of PM in saxony by size-segregated characterisation. J Atmos Chem. **55**(2), 103–130 (2006). doi:10.1007/s10874-006-9029-7

Hesterberg, R., Blatter, A., Fahrni, M., Rosset, M., Neftel, A., Eugster, W., Wanner, H.: Deposition of nitrogen-containing compounds to an extensively managed grassland in central Switzerland. Environ Pollut. **91**(1), 21–34 (1996). doi:10.1016/0269-7491(95)00036-Q

Hopke, P.K.: Review of receptor modeling methods for source apportionment. J Air Waste Manage Assoc. **66**(3), 237–259 (2016). doi:10.1080/10962247.2016.1140693

Hsu, Y.M., Clair, T.A.: Measurement of fine particulate matter water-soluble inorganic species and precursor gases in the Alberta Oil Sands region using an improved semicontinuous monitor. J Air Waste Manage Assoc. **65**(4), 423–435 (2015). doi:10.1080/10962247.2014.1001088

Huang, X.H.H., Bian, Q., Ng, W.M., Louie, P.K.K., Yu, J.Z.: Characterization of $PM_{2.5}$ major components and source investigation in suburban Hong Kong: A one year monitoring study. Aerosol Air Qual Res. **14**, 237–250 (2014)

Huang, Y., Li, L., Li, J., Wang, X., Chen, H., Chen, J., Yang, X., Gross, D.S., Wang, H., Qiao, L., Chen, C.: A case study of the highly time-resolved evolution of aerosol chemical and optical properties in urban Shanghai. China Atmos Chem Phys. **13**(8), 3931–3944 (2013). doi:10.5194/acp-13-3931-2013

Jansen, R.C., Chen, J.M., Hu, Y.J.: The impact of nonlocal ammonia on submicron particulate matter and visibility degradation in urban Shanghai. Adv Meteorol. (2014a). doi:10.1155/2014/534675

Jansen, R.C., Shi, Y., Chen, J.M., Hu, Y.J., Xu, C., Hong, S.M., Li, J., Zhang, M.: Using hourly measurements to explore the role of secondary inorganic aerosol in $PM_{2.5}$ during haze and fog in Hangzhou, China. Adv Atmos Sci. **31**(6), 1427–1434 (2014b). doi:10.1007/s00376-014-4042-2

Jones, A.M., Harrison, R.M.: Temporal trends in sulphate concentrations at European sites and relationships to sulphur dioxide. Atmos Environ. **45**(4), 873–882 (2011). doi:10.1016/j.atmosenv.2010.11.020

Katzman, T.L., Rutter, A.P., Schauer, J.J., Lough, G.C., Kolb, C.J., Van Klooster, S.: $PM_{2.5}$ and $PM_{10-2.5}$ compositions during wintertime episodes of elevated PM concentrations across the midwestern USA. Aerosol Air Qual Res. **10**(2), 140–U113 (2010). doi:10.4209/aaqr.2009.10.0063

Keck, L., Wittmaack, K.: Effect of filter type and temperature on volatilisation losses from ammonium salts in aerosol matter. Atmos Environ. **39**(22), 4093–4100 (2005). doi:10.1016/j.atmosenv.2005.03.029

Keuken, M.P., Schoonebeek, C.A.M., Vanwensveenlouter, A., Slanina, J.: Simultaneous sampling of NH_3, HNO_3, HCl, SO_2 and H_2O_2 in ambient air by a wet annular denuder system. Atmos Environ. **22**(11), 2541–2548 (1988). doi:10.1016/0004-6981(88)90486-6

Khezri, B., Mo, H., Yan, Z., Chong, S.L., Heng, A.K., Webster, R.D.: Simultaneous online monitoring of inorganic compounds in aerosols and gases in an industrialized area. Atmos Environ. **80**, 352–360 (2013). doi:10.1016/j.atmosenv.2013.08.008

Khlystov, A., Wyers, G.P., Slanina, J.: The steam-jet aerosol collector. Atmos Environ. **29**(17), 2229–2234 (1995). doi:10.1016/1352-2310(95)00180-7

Kleffmann, J., Wiesen, P.: Technical note: quantification of interferences of wet chemical HONO LOPAP measurements under simulated polar conditions. Atmos Chem Phys. **8**(22), 6813–6822 (2008)

Kong, L.D., Yang, Y.W., Zhang, S.Q., Zhao, X., Du, H.H., Fu, H.B., Zhang, S.C., Cheng, T.T., Yang, X., Chen, J.M., Wu, D., Shen, J.D., Hong, S.M., Jiao, L.: Observations of linear dependence between sulfate and nitrate in atmospheric particles. J Geophys Res-Atmos. **119**(1), 341–361 (2014). doi:10.1002/2013JD020222

Leng, C.P., Cheng, T.T., Chen, J.M., Zhang, R.J., Tao, J., Huang, G.H., Zha, S.P., Zhang, M.G., Fang, W., Li, X., Li, L.: Measurements of surface cloud condensation nuclei and aerosol activity in downtown Shanghai. Atmos Environ. **69**, 354–361 (2013). doi:10.1016/j.atmosenv.2012.12.021

Leng, C., Zhang, Q., Tao, J., Zhang, H., Zhang, D., Xu, C., Li, X., Kong, L., Cheng, T., Zhang, R., Yang, X., Chen, J., Qiao, L., Lou, S., Wang, H., Chen, C.: Impacts of new particle formation on aerosol cloud condensation nuclei (CCN) activity in Shanghai: case study. Atmos Chem Phys. **14**(20), 11353–11365 (2014a). doi:10.5194/acp-14-11353-2014

Leng, C., Zhang, Q., Zhang, D., Xu, C., Cheng, T., Zhang, R., Tao, J., Chen, J., Zha, S., Zhang, Y., Li, X., Kong, L., Gao, W.: Variations of cloud condensation nuclei (CCN) and aerosol activity during fog-haze episode: a case study from Shanghai. Atmos Chem Phys. **14**(22), 12499–12512 (2014b). doi:10.5194/acp-14-12499-2014

Li, L., Chen, J.M., Wang, L., Melluki, W., Zhou, H.R.: Aerosol single scattering albedo affected by chemical composition: an investigation using CRDS combined with MARGA. Atmos Res. **124**, 149–157 (2013). doi:10.1016/j.atmosres.2012.11.007

Li, H.Y., Han, Z.W., Cheng, T.T., Du, H.H., Kong, L.D., Chen, J.M., Zhang, R.J., Wang, W.J.: Agricultural fire impacts on the air quality of Shanghai during summer harvesttime. Aerosol Air Qual Res. **10**(2), 95–101 (2010). doi:10.4209/aaqr.2009.08.0049

Li, X., Rohrer, F., Hofzumahaus, A., Brauers, T., Haseler, R., Bohn, B., Broch, S., Fuchs, H., Gomm, S., Holland, F., Jager, J., Kaiser, J., Keutsch, F.N., Lohse, I., Lu, K.D., Tillmann, R., Wegener, R., Wolfe, G.M., Mentel, T.F., Kiendler-Scharr, A., Wahner, A.: Missing gas-phase source of HONO inferred from zeppelin measurements in the troposphere. Science. **344**(6181), 292–296 (2014). doi:10.1126/science.1248999

Liu, C.N., Lin, S.F., Awasthi, A., Tsai, C.J., Wu, Y.C., Chen, C.F.: Sampling and conditioning artifacts of $PM_{2.5}$ in filter-based samplers. Atmos Environ. **85**, 48–53 (2014). doi:10.1016/j.atmosenv.2013.11.075

Mair, P., Hofmann, E., Gruber, K., Hatzinger, R., Zeileis, A., Hornik, K.: Motivation, values, and work design as drivers of participation in the R open source project for statistical computing. P Natl Acad Sci USA. **112**(48), 14788–14792 (2015). doi:10.1073/pnas.1506047112

Makkonen, U., Virkkula, A., Hellen, H., Hemmila, M., Sund, J., Aijala, M., Ehn, M., Junninen, H., Keronen, P., Petaja, T., Worsnop, D.R., Kulmala, M., Hakola, H.: Semi-continuous gas and inorganic aerosol measurements at a boreal forest site: seasonal and diurnal cycles of NH_3, HONO and HNO_3. Boreal Environ Res. **19**, 311–328 (2014)

Makkonen, U., Virkkula, A., Mantykentta, J., Hakola, H., Keronen, P., Vakkari, V., Aalto, P.P.: Semi-continuous gas and inorganic aerosol measurements at a Finnish urban site: comparisons with filters, nitrogen in aerosol and gas phases, and aerosol acidity. Atmos Chem Phys. **12**(12), 5617–5631 (2012). doi:10.5194/acp-12-5617-2012

Malm, W.C., Johnson, C.E., Bresch, J.F.: Application of principal component analysis for purposes of identifying source-receptor relationships. In: Pace, T.G. (ed.) Transactions, Receptor Methods for Source Apportionment: Real World Issues and Applications, pp. 127–148. Air Pollution Control Association, Pittsburgh, PA (1985)

Markovic, M.Z., VandenBoer, T.C., Baker, K.R., Kelly, J.T., Murphy, J.G.: Measurements and modeling of the inorganic chemical composition of fine particulate matter and associated precursor gases in California's San Joaquin Valley during CalNex 2010. J Geophys Res-Atmos. **119**(11), 6853–6866 (2014). doi:10.1002/2013jd021408

Markovic, M.Z., VandenBoer, T.C., Murphy, J.G.: Characterization and optimization of an online system for the simultaneous measurement of atmospheric water-soluble constituents in the gas and particle phases. J Environ Monit. **14**(7), 1872–1884 (2012). doi:10.1039/C2em00004k

McCulloch, A., Aucott, M.L., Benkovitz, C.M., Graedel, T.E., Kleiman, G., Midgley, P.M., Li, Y.F.: Global emissions of hydrogen chloride and chloromethane from coal combustion, incineration and industrial activities: reactive chlorine emissions inventory. J Geophys Res-Atmos. **104**(D7), 8391–8403 (1999). doi:10.1029/1999jd900025

Mensah, A.A., Holzinger, R., Otjes, R., Trimborn, A., Mentel, T.F., ten Brink, H., Henzing, B., Kiendler-Scharr, A.: Aerosol chemical composition at Cabauw, The Netherlands as observed in two intensive periods in may 2008 and March 2009. Atmos Chem Phys. **12**(10), 4723–4742 (2012). doi:10.5194/acp-12-4723-2012

Metzger, S., Mihalopoulos, N., Lelieveld, J.: Importance of mineral cations and organics in gas-aerosol partitioning of reactive nitrogen compounds: case study based on MINOS results. Atmos Chem Phys. **6**, 2549–2567 (2006)

Michoud, V., Colomb, A., Borbon, A., Miet, K., Beekmann, M., Camredon, M., Aumont, B., Perrier, S., Zapf, P., Siour, G., Ait-Helal, W., Afif, C., Kukui, A., Furger, M., Dupont, J.C., Haeffelin, M., Doussin, J.F.: Study of the unknown HONO daytime source at a European suburban site during the MEGAPOLI summer and winter field campaigns. Atmos Chem Phys. **14**(6), 2805–2822 (2014). doi:10.5194/acp-14-2805-2014

Milford, C., Theobald, M.R., Nemitz, E., Hargreaves, K.J., Horvath, L., Raso, J., Dammgen, U., Neftel, A., Jones, S.K., Hensen, A., Loubet, B., Cellier, P., Sutton, M.A.: Ammonia fluxes in relation to cutting and fertilization of an intensively managed grassland derived from an inter-comparison of gradient measurements. Biogeosciences. **6**(5), 819–834 (2009). doi:10.5194/bg-6-819-2009

Möller, D.: Luft: Chemie, Physik, Biologie, Reinhaltung, Recht. Walter de Gruyter & Co, KG, Berlin and New York (2003)

Neuman, J.A., Huey, L.G., Ryerson, T.B., Fahey, D.W.: Study of inlet materials for sampling atmospheric nitric acid. Environ Sci Technol. **33**(7), 1133–1136 (1999). doi:10.1021/Es980767f

Neusüß, C., Pelzing, M., Plewka, A., Herrmann, H.: A new analytical approach for size-resolved speciation of organic compounds in atmospheric aerosol particles: methods and first results. J Geophys Res-Atmos. **105**(D4), 4513–4527 (2000). doi:10.1029/1999jd901038

Ng, N.L., Herndon, S.C., Trimborn, A., Canagaratna, M.R., Croteau, P.L., Onasch, T.B., Sueper, D., Worsnop, D.R., Zhang, Q., Sun, Y.L., Jayne, J.T.: An aerosol chemical speciation monitor (ACSM) for routine monitoring of the composition and mass concentrations of ambient aerosol. Aerosol Sci Technol. **45**(7), 780–794 (2011). doi:10.1080/02786826.2011.560211

Norman, M., Spirig, C., Wolff, V., Trebs, I., Flechard, C., Wisthaler, A., Schnitzhofer, R., Hansel, A., Neftel, A.: Intercomparison of ammonia measurement techniques at an intensively managed grassland site (Oensingen, Switzerland). Atmos Chem Phys. **9**(8), 2635–2645 (2009)

Ocskay, R., Salma, I., Wang, W., Maenhaut, W.: Characterization and diurnal variation of size-resolved inorganic water-soluble ions at a rural background site. J Environ Monit. **8**(2), 300–306 (2006). doi:10.1039/b513915e

Orsini, D.A., Ma, Y.L., Sullivan, A., Sierau, B., Baumann, K., Weber, R.J.: Refinements to the particle-into-liquid sampler (PILS) for ground and airborne measurements of water soluble aerosol composition. Atmos Environ. **37**(9–10), 1243–1259 (2003). doi:10.1016/S1352-2310(02)01015-4

Pekney, N.J., Davidson, C.I., Zhou, L.M., Hopke, P.K.: Application of PSCF and CPF to PMF-modeled sources of $PM_{2.5}$ in Pittsburgh. Aerosol Sci Technol. **40**(10), 952–961 (2006). doi:10.1080/02786820500543324

Perrino, C., Canepari, S., Pappalardo, S., Marconi, E.: Time-resolved measurements of water-soluble ions and elements in atmospheric particulate matter for the characterization of local and long-range transport events. Chemosphere. **80**(11), 1291–1300 (2010). doi:10.1016/j.chemosphere.2010.06.050

Peter, J.R., Siems, S.T., Jensen, J.B., Gras, J.L., Ishizaka, Y., Hacker, J.M.: Airborne observations of the effect of a cold front on the aerosol particle size distribution and new particle formation. Q J R Meteorol Soc. **136**, 944–961 (2010). doi:10.1002/qj.515

Phillips, G.J., Makkonen, U., Schuster, G., Sobanski, N., Hakola, H., Crowley, J.N.: The detection of nocturnal N_2O_5 as HNO_3 by alkali- and aqueous-denuder techniques. Atmos Meas Tech. **6**(2), 231–237 (2013). doi:10.5194/amt-6-231-2013

Pinto, J.P., Dibb, J., Lee, B.H., Rappengluck, B., Wood, E.C., Levy, M., Zhang, R.Y., Lefer, B., Ren, X.R., Stutz, J., Tsai, C., Ackermann, L., Golovko, J., Herndon, S.C., Oakes, M., Meng, Q.Y., Munger, J.W., Zahniser, M., Zheng, J.: Intercomparison of field measurements of nitrous acid (HONO) during the SHARP campaign. J Geophys Res-Atmos. **119**(9), 5583–5601 (2014). doi:10.1002/2013jd020287

Pio, C.A., Harrison, R.M.: The equilibrium of ammonium-chloride aerosol with gaseous hydrochloric-acid and ammonia under tropospheric conditions. Atmos Environ. **21**(5), 1243–1246 (1987). doi:10.1016/0004-6981(87)90253-8

Pio, C.A., Lopes, D.A.: Chlorine loss from marine aerosol in a coastal atmosphere. J Geophys Res-Atmos. **103**(D19), 25263–25272 (1998). doi:10.1029/98jd02088

Plessow, K., Spindler, G., Zimmermann, F., Matschullat, K.: Seasonal variations and interactions of N-containing gases and particles over a coniferous forest, Saxony. Germany Atmos Environ. **39**(37), 6995–7007 (2005). doi:10.1016/j.atmosenv.2005.07.046

Poulain, L., Birmili, W., Canonaco, F., Crippa, M., Wu, Z.J., Nordmann, S., Spindler, G., Prévôt, A.S.H., Wiedensohler, A., Herrmann, H.: Chemical mass balance of 300 °C non-volatile particles at the tropospheric research site Melpitz. Germany Atmos Chem Phys. **14**(18), 10145–10162 (2014). doi:10.5194/acp-14-10145-2014

Poulain, L., Spindler, G., Birmili, W., Plass-Dülmer, C., Wiedensohler, A., Herrmann, H.: Seasonal and diurnal variations of particulate nitrate and organic matter at the IfT research station Melpitz. Atmos Chem Phys. **11**(24), 12579–12599 (2011). doi:10.5194/acp-11-12579-2011

Rogula-Kozlowska, W.: Chemical composition and mass closure of ambient particulate matter at a crossroads and a highway in Katowice. Poland Environ Prot Eng. **41**(2), 15–29 (2015). doi:10.5277/epe150202

Rumsey, I.C., Cowen, K.A., Walker, J.T., Kelly, T.J., Hanft, E.A., Mishoe, K., Rogers, C., Proost, R., Beachley, G.M., Lear, G., Frelink, T., Otjes, R.P.: An assessment of the performance of the monitor for AeRosols and GAses in ambient air (MARGA): a semi-continuous method for soluble compounds. Atmos Chem Phys. **14**, 5639–5658 (2014)

Rumsey, I.C., Walker, J.T.: Application of an online ion-chromatography-based instrument for gradient flux measurements of speciated nitrogen and sulfur. Atmos Meas Tech. **9**(6), 2581–2592 (2016). doi:10.5194/amt-9-2581-2016

Schaap, M., Otjes, R.P., Weijers, E.P.: Illustrating the benefit of using hourly monitoring data on secondary inorganic aerosol and its precursors for model evaluation. Atmos Chem Phys. **11**(21), 11041–11053 (2011). doi:10.5194/acp-11-11041-2011

Schaap, M., Spindler, G., Schulz, M., Acker, K., Maenhaut, W., Berner, A., Wieprecht, W., Streit, N., Müller, K., Brüggemann, E., Chi, X., Putaud, J.P., Hitzenberger, R., Puxbaum, H., Baltensperger, U., ten Brink, H.: Artefacts in the sampling of nitrate studied in the "INTERCOMP" campaigns of EUROTRAC-AEROSOL. Atmos Environ. **38**(38), 6487–6496 (2004). doi:10.1016/j.atmosenv.2004.08.026

Schwab, J.J., Li, Y.Q., Bae, M.S., Demerjian, K.L., Hou, J., Zhou, X.L., Jensen, B., Pryor, S.C.: A laboratory intercomparison of real-time gaseous ammonia measurement methods. Environ Sci Technol. **41**(24), 8412–8419 (2007). doi:10.1021/es070354r

Seinfeld, J.H., Pandis, S.N.: Atmospheric chemistry and physics - from air pollution to climate change, vol. 2. John Wiley & Sons, Inc., Hoboken, New Jersey (2006)

Shi, Y., Chen, J.M., Hu, D.W., Wang, L., Yang, X., Wang, X.M.: Airborne submicron particulate (PM_1) pollution in Shanghai, China: chemical variability, formation/dissociation of associated semi-volatile components and the impacts on visibility. Sci Total Environ. **473**, 199–206 (2014). doi:10.1016/j.scitotenv.2013.12.024

Slanina, J., ten Brink, H.M., Otjes, R.P., Even, A., Jongejan, P., Khlystov, A., Waijers-Ijpelaan, A., Hu, M.: The continuous analysis of nitrate and ammonium in aerosols by the steam jet aerosol collector (SJAC): extension and validation of the methodology. Atmos Environ. **35**(13), 2319–2330 (2001). doi:10.1016/S1352-2310(00)00556-2

Sorooshian, A., Brechtel, F.J., Ma, Y.L., Weber, R.J., Corless, A., Flagan, R.C., Seinfeld, J.H.: Modeling and characterization of a particle-into-liquid sampler (PILS). Aerosol Sci Technol. **40**(6), 396–409 (2006). doi:10.1080/02786820600632282

Spataro, F., Ianniello, A.: Sources of atmospheric nitrous acid: state of the science, current research needs, and future prospects. J Air Waste Manage Assoc. **64**(11), 1232–1250 (2014). doi:10.1080/10962247.2014.952846

Spindler, G., Brüggemann, E., Gnauk, T., Grüner, A., Müller, K., Herrmann, H.: A four-year size-segregated characterization study of particles PM_{10}, $PM_{2.5}$ and PM_1 depending on air mass origin at Melpitz. Atmos Environ. **44**(2), 164–173 (2010). doi:10.1016/j.atmosenv.2009.10.015

Spindler, G., Grüner, A., Müller, K., Schlimper, S., Herrmann, H.: Long-term size-segregated particle (PM_{10}, $PM_{2.5}$, PM_1) characterization study at Melpitz - influence of air mass inflow, weather conditions and season. J Atmos Chem. **70**(2), 165–195 (2013). doi:10.1007/s10874-013-9263-8

Spindler, G., Hesper, J., Brüggemann, E., Dubois, R., Müller, T., Herrmann, H.: Wet annular denuder measurements of nitrous acid: laboratory study of the artefact reaction of NO_2 with S(IV) in aqueous solution and comparison with field measurements. Atmos Environ. **37**(19), 2643–2662 (2003). doi:10.1016/S1352-2310(03)00209-7

Spindler, G., Müller, K., Brüggemann, E., Gnauk, T., Herrmann, H.: Long-term size-segregated characterization of PM_{10}, $PM_{2.5}$, and PM_1 at the IfT research station Melpitz downwind of Leipzig (Germany) using high and low-volume filter samplers. Atmos Environ. **38**(31), 5333–5347 (2004). doi:10.1016/j.atmosenv.2003.12.047

Spindler, G., Müller, K., Herrmann, H.: Main particulate matter components in Saxony (Germany) - trends and sampling aspects. Environ Sci Pollut R. **6**(2), 89–94 (1999). doi:10.1007/Bf02987559

Squizzato, S., Masiol, M., Brunelli, A., Pistollato, S., Tarabotti, E., Rampazzo, G., Pavoni, B.: Factors determining the formation of secondary inorganic aerosol: a case study in the Po Valley (Italy). Atmos Chem Phys. **13**(4), 1927–1939 (2013). doi:10.5194/acp-13-1927-2013

Stein, A.F., Draxler, R.R., Rolph, G.D., Stunder, B.J.B., Cohen, M.D., Ngan, F.: NOAA's HYSPLIT atmospheric transport and dispersion modeling system. B Am Meteorol Soc. **96**(12), 2059–2077 (2015). doi:10.1175/Bams-D-14-00110.1

Stutz, J., Oh, H.J., Whitlow, S.I., Anderson, C., Dibb, J.E., Flynn, J.H., Rappengluck, B., Lefer, B.: Simultaneous DOAS and mist-chamber IC measurements of HONO in Houston. TX Atmos Environ. **44**(33), 4090–4098 (2010). doi:10.1016/j.atmosenv.2009.02.003

Sudheer, A.K., Rengarajan, R.: Time-resolved inorganic chemical composition of fine aerosol and associated precursor gases over an urban environment in western India: gas-aerosol equilibrium characteristics. Atmos Environ. **109**, 217–227 (2015). doi:10.1016/j.atmosenv.2015.03.028

Sudheer, A.K., Rengarajan, R., Deka, D., Bhushan, R., Singh, S.K., Aslam, M.Y.: Diurnal and seasonal characteristics of aerosol ionic constituents over an urban location in western India: secondary aerosol formation and meteorological influence. Aerosol Air Qual Res. **14**(6), 1701–U1527 (2014). doi:10.4209/aaqr.2013.09.0288

Tan, H.B., Cai, M.F., Fan, Q., Liu, L., Li, F., Chan, P.W., Deng, X.J., Wu, D.: An analysis of aerosol liquid water content and related impact factors in Pearl River Delta. Sci Total Environ. **579**, 1822–1830 (2017). doi:10.1016/j.scitotenv.2016.11.167

Tang, Y.B., Li, Z.H., Yang, Y.I., Ma, D.J., Ji, H.J.: Effect of inorganic chloride on spontaneous combustion of coal. J S Afr I Min Metall. **115**(2), 87–92 (2015)

ten Brink, H., Otjes, R., Jongejan, P., Kos, G.: Monitoring of the ratio of nitrate to sulphate in size-segregated submicron aerosol in the Netherlands. Atmos Res. **92**, 270–276 (2009)

ten Brink, H., Otjes, R., Jongejan, P., Slanina, S.: An instrument for semi-continuous monitoring of the size-distribution of nitrate, ammonium, sulphate and chloride in aerosol. Atmos Environ. **41**, 2768–2779 (2007)

Thomas, R.M., Trebs, I., Otjes, R., Jongejan, P.A.C., Ten Brink, H., Phillips, G., Kortner, M., Meixner, F.X., Nemitz, E.: An automated analyzer to measure surface-atmosphere exchange fluxes of water soluble inorganic aerosol compounds and reactive trace gases. Environ Sci Technol. **43**(5), 1412–1418 (2009). doi:10.1021/Es8019403

Tilgner, A., Schöne, L., Bräuer, P., van Pinxteren, D., Hoffmann, E., Spindler, G., Styler, S.A., Mertes, S., Birmili, W., Otto, R., Merkel, M., Weinhold, K., Wiedensohler, A., Deneke, H., Schrödner, R., Wolke, R., Schneider, J., Haunold, W., Engel, A., Weber, A., Herrmann, H.: Comprehensive assessment of meteorological conditions and airflow connectivity during HCCT-2010. Atmos Chem Phys. **14**(17), 9105–9128 (2014). doi:10.5194/acp-14-9105-2014

Trebs, I., Meixner, F.X., Slanina, J., Otjes, R., Jongejan, P., Andreae, M.O.: Real-time measurements of ammonia, acidic trace gases and water-soluble inorganic aerosol species at a rural site in the Amazon Basin. Atmos Chem Phys. **4**, 967–987 (2004)

Twigg, M.M., Di Marco, C.F., Leeson, S., van Dijk, N., Jones, M.R., Leith, I.D., Morrison, E., Coyle, M., Proost, R., Peeters, A.N.M., Lemon, E., Frelink, T., Braban, C.F., Nemitz, E., Cape, J.N.: Water soluble aerosols and gases at a UK background site - Part 1: Controls of $PM_{2.5}$ and PM_{10} aerosol composition. Atmos Chem Phys. **15**(14), 8131–8145 (2015). doi:10.5194/acp-15-8131-2015

VandenBoer, T.C., Petroff, A., Markovic, M.Z., Murphy, J.G.: Size distribution of alkyl amines in continental particulate matter and their online detection in the gas and particle phase. Atmos Chem Phys. **11**(9), 4319–4332 (2011). doi:10.5194/acp-11-4319-2011

VandenBoer, T.C., Young, C.J., Talukdar, R.K., Markovic, M.Z., Brown, S.S., Roberts, J.M., Murphy, J.G.: Nocturnal loss and daytime source of nitrous acid through reactive uptake and displacement. Nat Geosci. **8**(1), 55–60 (2014). doi:10.1038/ngeo2298

Vecchi, R., Marcazzan, G., Valli, G.: A study on nighttime-daytime PM_{10} concentration and elemental composition in relation to atmospheric dispersion in the urban area of Milan (Italy). Atmos Environ. **41**(10), 2136–2144 (2007). doi:10.1016/j.atmonsenv.2006.10.069

Volten, H., Bergwerff, J.B., Haaima, M., Lolkema, D.E., Berkhout, A.J.C., van der Hoff, G.R., Potma, C.J.M., Kruit, R.J.W., van Pul, W.A.J., Swart, D.P.J.: Two instruments based on differential optical absorption spectroscopy (DOAS) to measure accurate ammonia concentrations in the atmosphere. Atmos Meas Tech. **5**(2), 413–427 (2012). doi:10.5194/amt-5-413-2012

von Bobrutzki, K., Braban, C.F., Famulari, D., Jones, S.K., Blackall, T., Smith, T.E.L., Blom, M., Coe, H., Gallagher, M., Ghalaieny, M., McGillen, M.R., Percival, C.J., Whitehead, J.D., Ellis, R., Murphy, J., Mohacsi, A., Pogany, A., Junninen, H., Rantanen, S., Sutton, M.A., Nemitz, E.: Field inter-comparison of eleven atmospheric ammonia measurement techniques. Atmos Meas Tech. **3**(1), 91–112 (2010). doi:10.5194/amt-3-91-2010

Wang, L., Du, H.H., Chen, J.M., Zhang, M., Huang, X.Y., Tan, H.B., Kong, L.D., Geng, F.H.: Consecutive transport of anthropogenic air masses and dust storm plume: two case events at Shanghai. China Atmos Res. **127**, 22–33 (2013a). doi:10.1016/j.atmosres.2013.02.011

Wang, H.L., Qiao, L.P., Lou, S.R., Zhou, M., Chen, J.M., Wang, Q., Tao, S.K., Chen, C.H., Huang, H.Y., Li, L., Huang, C.: PM2.5 pollution episode and its contributors from 2011 to 2013 in urban Shanghai, China. Atmos Environ. **123**, 298–305 (2015). doi:10.1016/j.atmosenv.2015.08.018

Wang, H.L., Qiao, L.P., Lou, S.R., Zhou, M., Ding, A.J., Huang, H.Y., Chen, J.M., Wang, Q., Tao, S., Chen, C.H., Li, L., Huang, C.: Chemical composition of $PM_{2.5}$ and meteorological impact among three years in urban Shanghai, China. J Clean Prod. **112**, 1302–1311 (2016). doi:10.1016/j.jclepro.2015.04.099

Wang, S.S., Zhou, R., Zhao, H., Wang, Z.R., Chen, L.M., Zhou, B.: Long-term observation of atmospheric nitrous acid (HONO) and its implication to local NO_2 levels in Shanghai. China Atmos Environ. **77**, 718–724 (2013b). doi:10.1016/j.atmosenv.2013.05.071

Wen, L., Chen, J.: Severe aerosol pollution derived from fireworks: a case in Jinan. China JSM Environmental Science & Ecology. **1**(1), 1004 (2013)

Whitehead, J.D., Twigg, M., Famulari, D., Nemitz, E., Sutton, M.A., Gallagher, M.W., Fowler, D.: Evaluation of laser absorption spectroscopic techniques for eddy covariance flux measurements of ammonia. Environ Sci Technol. **42**(6), 2041–2046 (2008). doi:10.1021/es071596u

Wyers, G.P., Otjes, R.P., Slanina, J.: A continuous-flow denuder for the measurement of ambient concentrations and surface-exchange fluxes of ammonia. Atmos Environ a-Gen. **27**(13), 2085–2090 (1993). doi:10.1016/0960-1686(93)90280-C

Xie, Y., Berkowitz, C.M.: The use of conditional probability functions and potential source contribution functions to identify source regions and advection pathways of hydrocarbon emissions in Houston. Texas Atmos Environ. **41**(28), 5831–5847 (2007). doi:10.1016/j.atmosenv.2007.03.049

Xie, W., Pan, W.L., Shen, D., Pan, W.P., Riley, J.T.: Studies of chlorine and sulfur behavior during coal combustion in an AFBC system. Abstr Pap Am Chem S. **213**, 127-FUEL (1997)

Xu, W.Y., Zhao, C.S., Ran, L., Lin, W.L., Yan, P., Xu, X.B.: SO_2 noontime-peak phenomenon in the North China plain. Atmos Chem Phys. **14**(15), 7757–7768 (2014). doi:10.5194/acp-14-7757-2014

Ye, X.N., Ma, Z., Zhang, J.C., Du, H.H., Chen, J.M., Chen, H., Yang, X., Gao, W., Geng, F.H.: Important role of ammonia on haze formation in Shanghai. Environ Res Lett. **6**(2), (2011). doi:10.1088/1748-9326/6/2/024019

Ye, X.N., Tang, C., Yin, Z., Chen, J.M., Ma, Z., Kong, L.D., Yang, X., Gao, W., Geng, F.H.: Hygroscopic growth of urban aerosol particles during the 2009 mirage-Shanghai campaign. Atmos Environ. **64**, 263–269 (2013). doi:10.1016/j.atmosenv.2012.09.064

Zhang, M., Chen, J.M., Chen, X.Y., Cheng, T.T., Zhang, Y.L., Zhang, H.F., Ding, A.J., Wang, M., Mellouki, A.: Urban aerosol characteristics during the World expo 2010 in Shanghai. Aerosol Air Qual Res. **13**(1), 36–48 (2013). doi:10.4209/aaqr.2012.02.0024

Zhou, Y., Huang, X.H., Bian, Q.J., Griffith, S.M., Louie, P.K.K., Yu, J.Z.: Sources and atmospheric processes impacting oxalate at a suburban coastal site in Hong Kong: Insights inferred from 1year hourly measurements. J Geophys Res-Atmos. **120**(18), 9772–9788 (2015). doi:10.1002/2015JD023531

Zhou, Y., Huang, X.H.H., Griffith, S.M., Li, M., Li, L., Zhou, Z., Wu, C., Meng, J.W., Chan, C.K., Louie, P.K.K., Yu, J.Z.: A field measurement based scaling approach for quantification of major ions, organic carbon, and elemental carbon using a single particle aerosol mass spectrometer. Atmos Environ. **143**, 300–312 (2016). doi:10.1016/j.atmosenv.2016.08.054

Zhou, G.Q., Yang, F., Geng, F.H., Xu, J.M., Yang, X., Tie, X.X.: Measuring and modeling aerosol: relationship with haze events in Shanghai. China Aerosol Air Qual Res. **14**(3), 783–792 (2014). doi:10.4209/aaqr.2013.01.0019